GRID INTEGRATION OF E-MOBILITY IN A WIRELESS WAY

-IP4: HARNESSING DISRUPTIVE TECHNOLOGIES FOR EARTHQUAKE RESILIENCE

QuakeCoRE
NZ Centre for Earthquake Resilience
Te Hiranga Rū

Innovative Smart Grid Technologies 2023 ISGT Asia

Yuan Liu

The University of Auckland
Department of Electrical, Computer and Software Engineering

CONTENTS

Background

This IP4 program will identify how transformational (i.e. order of magnitude) advancements in NZs infrastructure resilience can be achieved through strategic adoption of disruptive technologies, via government and market-led initiatives. A central hypothesis is that rapid adoption of several disruptive technologies (e.g. distributed solar power, autonomous transport, and a sensing society) will result in a significantly greater resilience gain than the conventional wisdom of incremental investment to improve existing asset classes (e.g. centralized transmission networks, physical logistics, significantly increased public awareness and preparedness).

The following key questions needs to be understood:

•What is the failure hierarchy of a renewable distributed energy system in seismic events?
•How should existing asset management investment occur to provide resilience during the transition to a renewable and distributed energy system?
•How can real-time sensing enable early detection of network degradation pre-event, and situational awareness in the immediate post-event environment for rapid restoration?
•How do individual utility networks develop resilience to externality risks and avoid contagion?
•How does the trade-off in electrification of transportation, reducing vulnerable reliance on liquid fuels, but increasing resilience requirements for electricity, play out over time?
•How will autonomous transportation modes function in a beyond business-as-usual environment? (e.g. physically damaged roads, disrupted electrical systems)

Why EV?

Automobile Exhaust air Pollution

Depletion of fossil resources

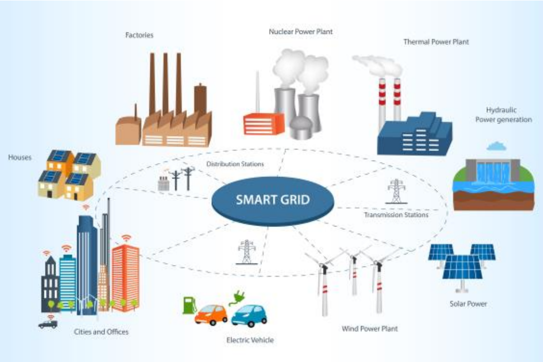

Development of smart/distribution grid

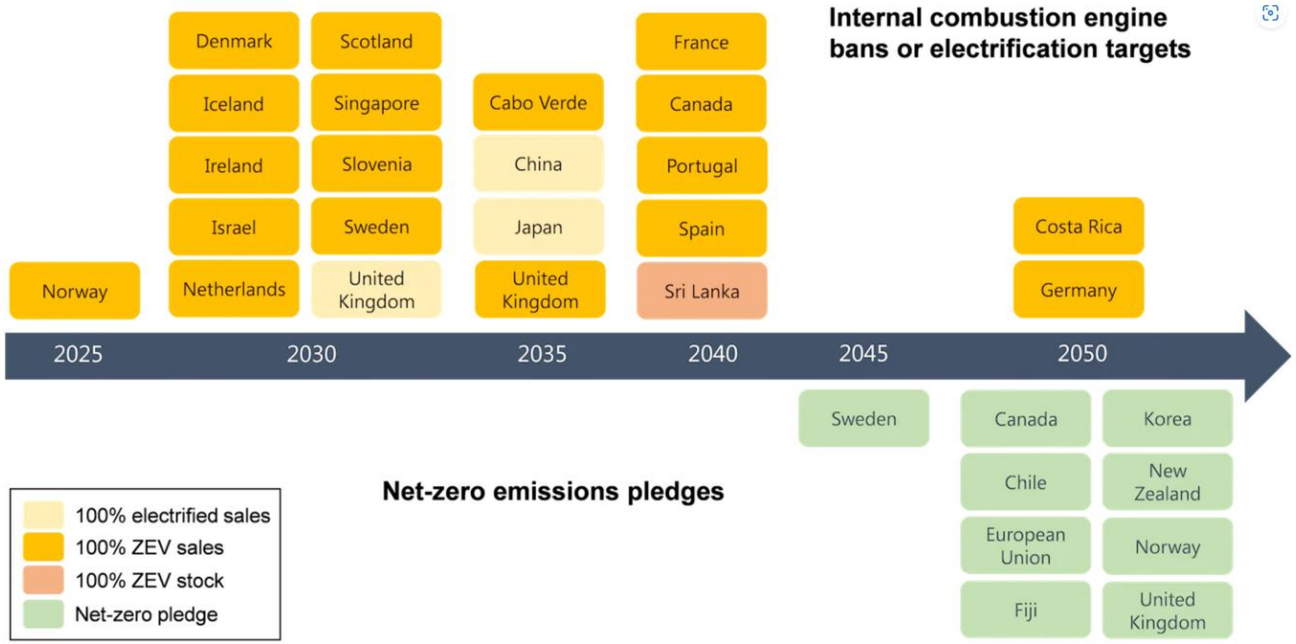

Fig. 1. International electrification targets

NZ government policy

Charging Our Future: National electric vehicle charging strategy for Aotearoa New Zealand 2023-2035

The long-term vision and strategic plan for Aotearoa New Zealand's electric vehicle (EV) charging infrastructure

V2G

Vehicle-to-grid, or **V2G for short**, is a technology that enables energy to be pushed back to the power grid from the battery of an electric vehicle (EV). With V2G technology, an EV battery can be discharged based on different signals — such as energy production or consumption nearby.

V2G technology **enables the flow of the energy between the car's battery and the grid.**

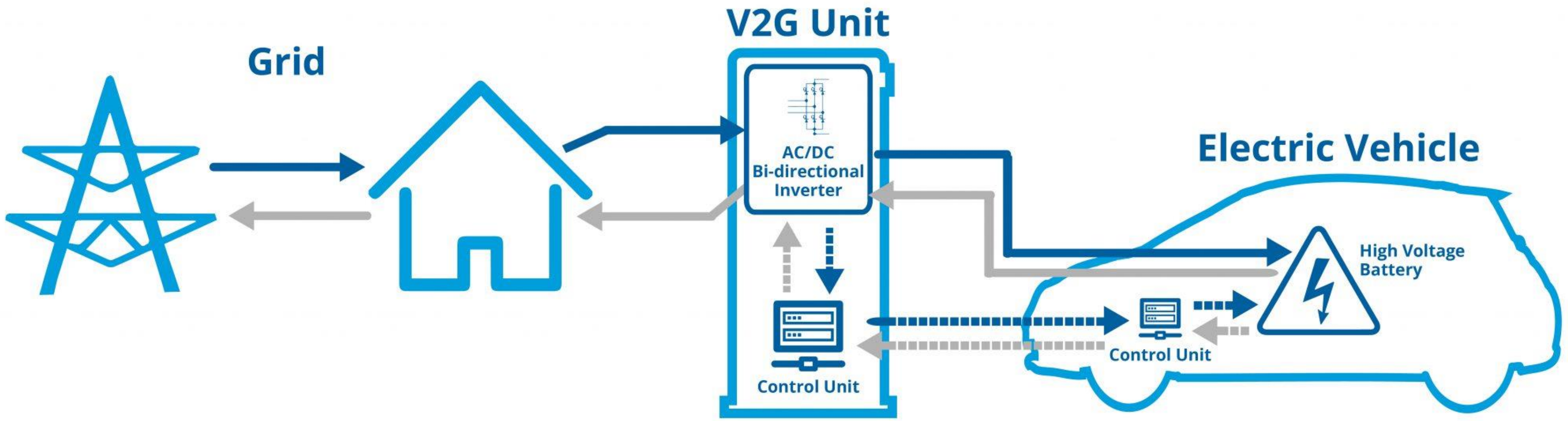

Fig. 2. A grid connected bi-directional V2G

WV2G

Wireless Vehicle-to-grid, or **WV2G for short**, is a technology that enables energy to be pushed back to the power grid from the battery of an electric vehicle (EV) wirelessly.

Bi-directional WV2G

AC power from the grid is converted to direct current (DC) voltage that is stored in the car's battery while charging. Then, EV drivers can access the power in the battery to power a home or add power back to the electricity grid. For this to happen, the power is converted from DC to AC electricity. A converter in the vehicle or in the charger itself performs this function, which takes the energy stored in the car's battery and push it back to the power grid wirelessly.

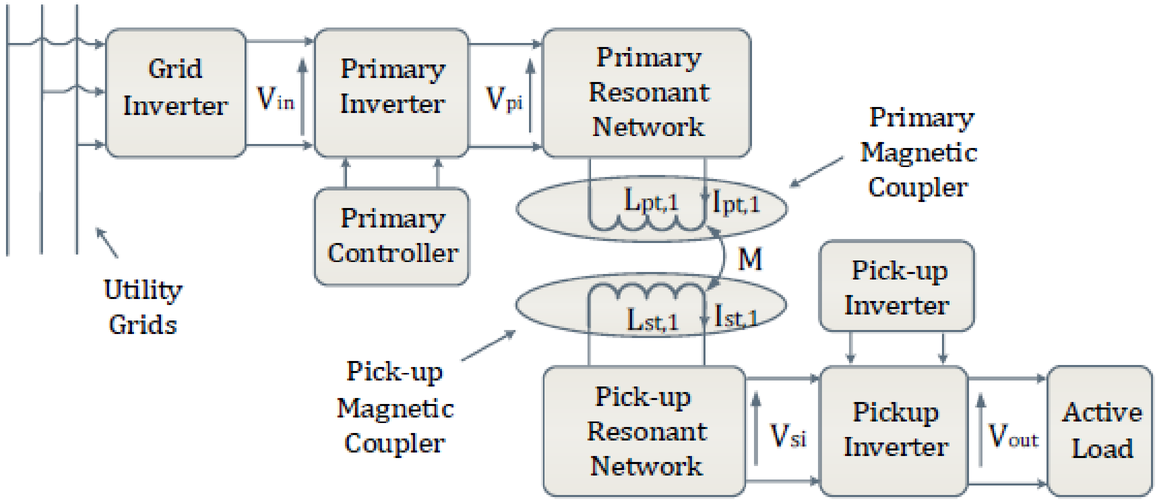

Fig. 3. A diagram of grid connected bi-directional wireless V2G

Why WV2G?

Eliminate charging-wire messes

Reduce electric shocks

Convenient and safe for the user

Bi-directional WPT

Advantages of Bi-directional Wireless power transfer

- Vehicle to Grid (V2G)/ Grid to Vehicle (G2V)
- Vehicle to X (Vehicle to Home (V2H), Vehicle to Load (V2L), Vehicle to Vehicle (V2V))
- Backup Power During Blackouts
- Greater Spatial freedom between the power source and the device
- Eliminating charging cords for compact design and adoption in harsh environments.

Inductive Power Transfer (IPT)

Basic structure and working principle:

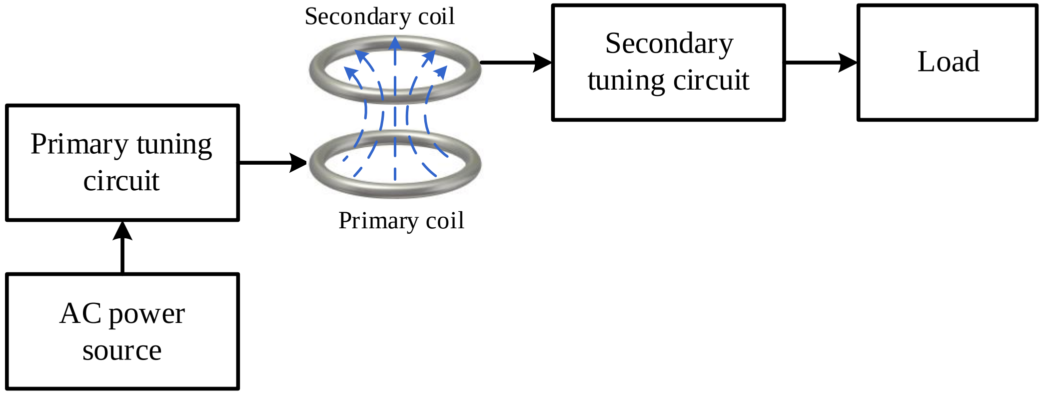

Fig. 4. Block diagram of a typical IPT system

Features:

- Eliminating charging cords for compact and wearable devices.
- Preventing corrosion and sparkling in coal mine and deep sea.
- Reducing costs associated with maintaining mechanical connectors.
- Allowing for greater spatial freedom between the power source and the charging device, and multiple-device charging.

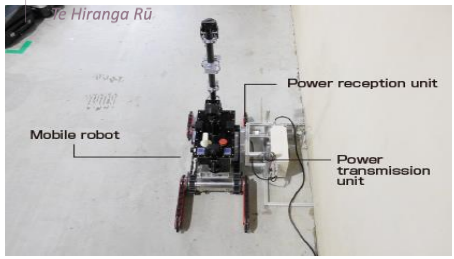

TDK’s 200w robot by IPT Robot

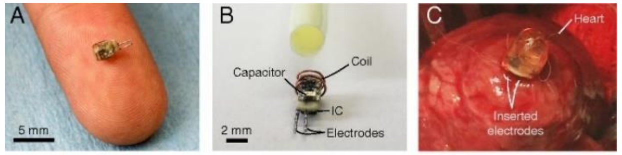

IPT to deep-tissue micro-implants

Spansive wireless charger

Wireless charging for home appliances

EV from Witricity

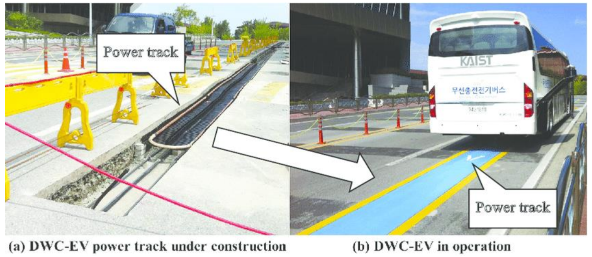

Online Electric Vehicle from KAIST

Road for dynamic charging in UK

Fig. 5. Applications of IPT systems

IPT – based EV

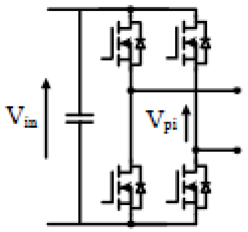

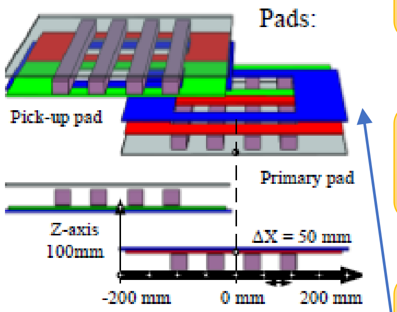

Grid converter
(AC-DC)

Primary/Pickup converter
(DC-High frequency AC)

Compensation network
(Filtering, resonating)

Couplers design
(Coupled coils)

Voltage regulation

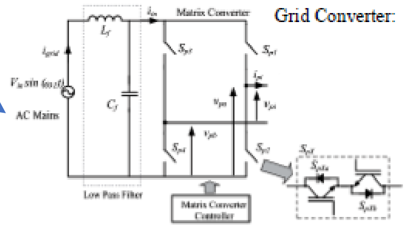

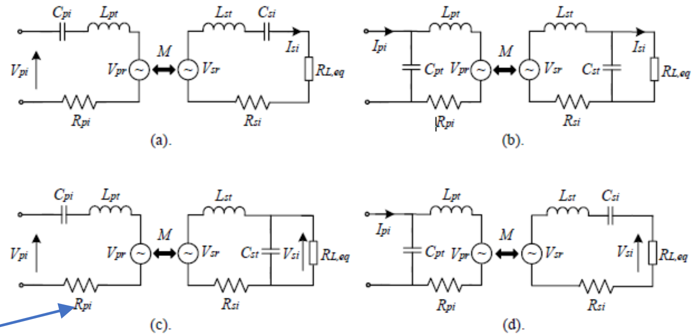

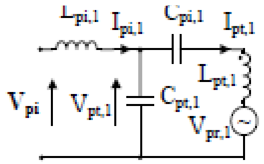

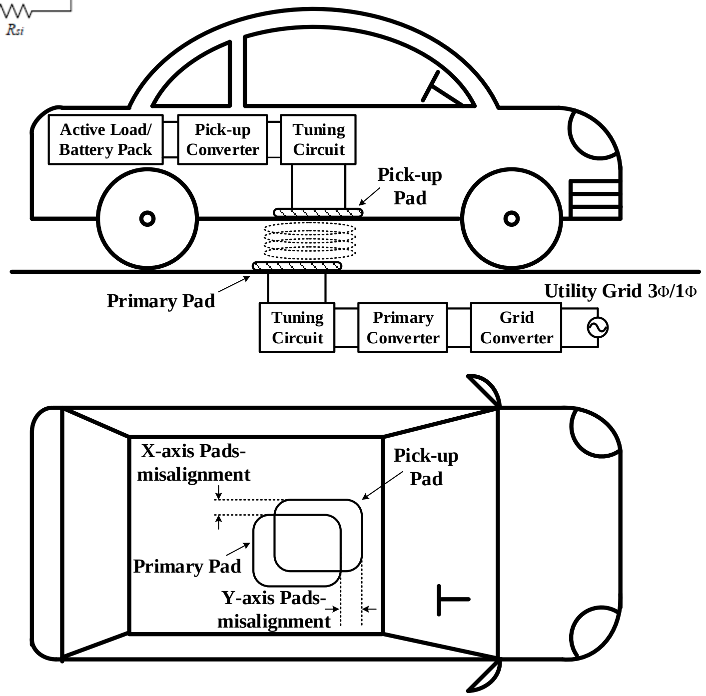

Fig. 6. A Typical IPT-based EV

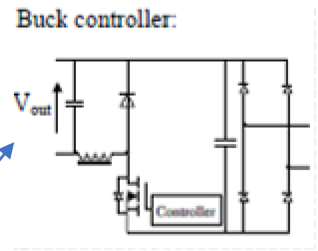

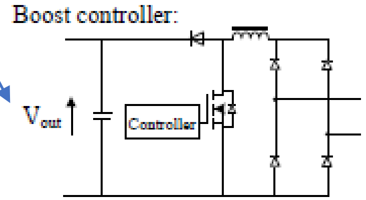

Capacitive Power Transfer (CPT)

Basic structure and working principle:

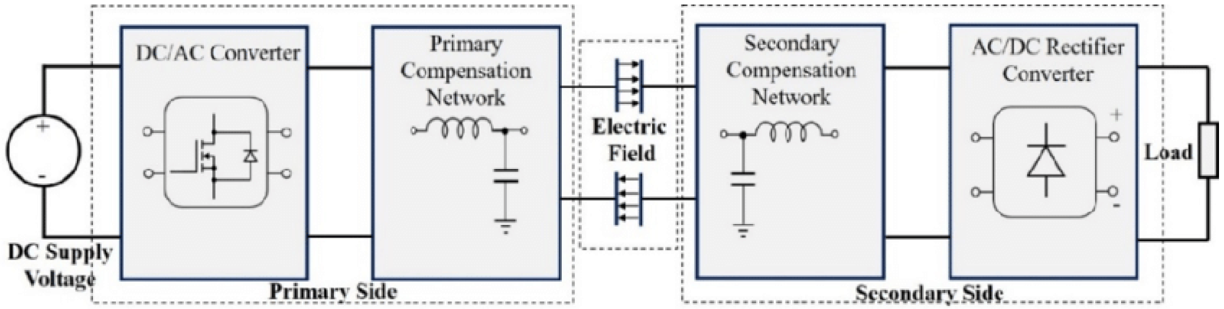

Fig. 7. Block diagram of a typical CPT system

Features:

- Eliminating charging cords for compact and wearable devices.
- Light, compact structure and reduced costs compared with IPT coil couplers.
- Allowing for greater spatial freedom between the power source and the charging device, and multiple-device charging.

Challenges:

- Complexity in modelling the couplers.
- Sensitivity due to high frequency.
- Dependency on the material of the couplers and ambient environment.

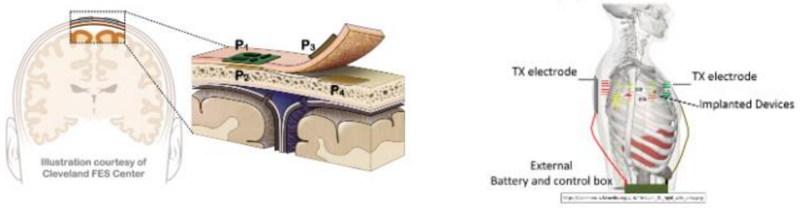

CPT to deep-tissue micro-implants

Hitachi CPT charger

CPT charging for drones

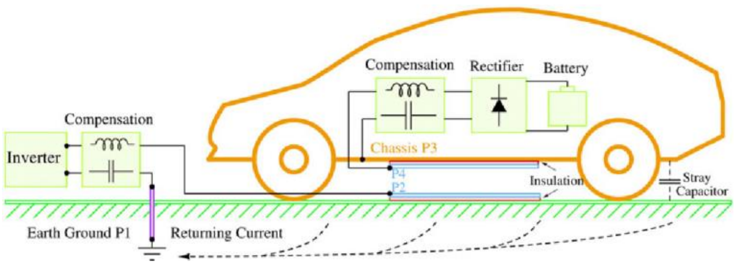

CPT for Static EV charging

Fig. 8. Applications of CPT systems

CPT – based EV

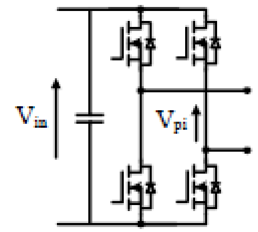

Grid converter (AC-DC)

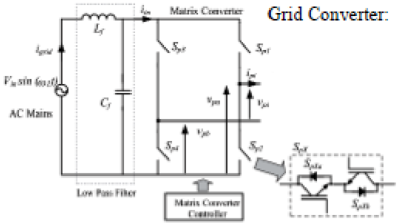

Primary/Pickup converter (DC-High frequency AC)

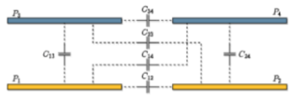

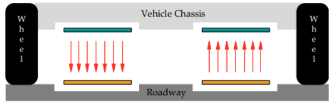

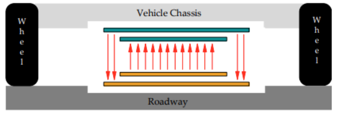

Compensation network (Filtering, resonating)

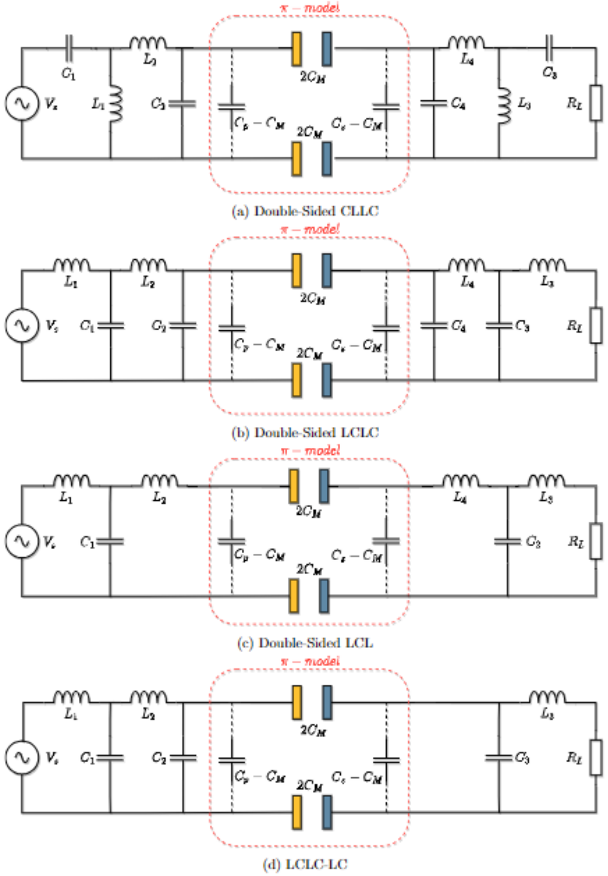

Couplers design (Coupled plates)

Voltage regulation

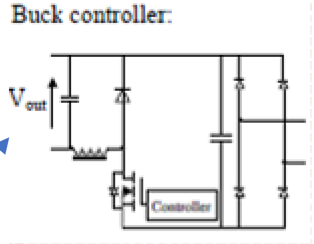

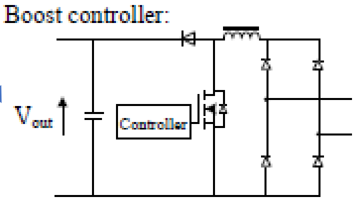

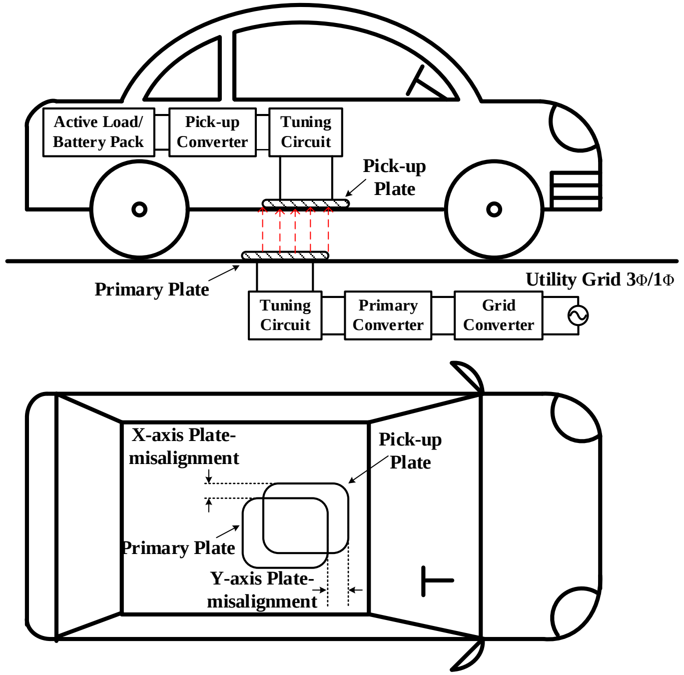

Fig. 9. A Typical CPT-based EV

Present Challenges of WV2G Systems

Requirements:

- High power
- High efficiency
- Compact structure on Pick-up (EV) side

Challenges:

- Weak coupling → High Current in coupled coils (IPT)
  → High Voltage on coupled plates (CPT)
- Power and Efficiency drop due to misalignments

Research Objectives

Possible topics:

- New compensation topologies
- New control methods
- Integration of EVs to other smart/micro-grids

Ph. D research

Two-coil IPT setup

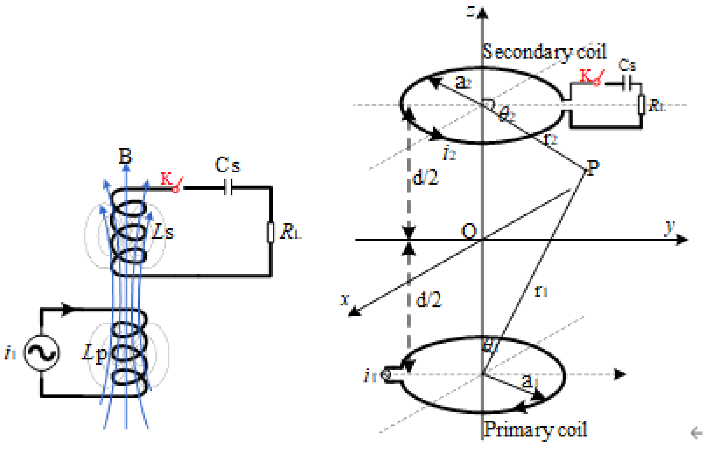

(a) (b)

Fig. 10. The researched IPT system. (a) A two-coil coupled IPT system, (b) The analysed two-coil setup

- The expressions of magnetic and electric field in the near field region

$$\mathbf{H}_1 = H_{1r}\vec{r}_1 + H_{1\theta}\vec{\theta}_1$$

$$H_{1r} = \frac{a_1^2}{2r_1^3} I_1 e^{-j(\omega t + kr_1)} \cos\theta_1$$

$$H_{1\theta} = \frac{a_1^2}{4r_1^3} I_1 e^{-j(\omega t + kr_1)} \sin\theta_1$$

$$\mathbf{H}_2 = H_{2r}\vec{r}_2 + H_{2\theta}\vec{\theta}_2$$

$$H_{2r} = \frac{a_2^2}{2r_2^3} I_2 e^{-j(\omega t + kr_2 + \phi)} \cos\theta_2$$

$$H_{2\theta} = \frac{a_2^2}{4r_2^3} I_2 e^{-j(\omega t + kr_2 + \phi)} \sin\theta_2$$

$$\mathbf{E}_1 = E_{1\phi}\vec{\phi}$$

$$E_{1\phi} = -j\eta \frac{ka_1^2}{4r_1^2} I_1 e^{-j(\omega t + kr_1)} \sin\theta_1$$

$$\mathbf{E}_2 = E_{2\phi}\vec{\phi}$$

$$E_{2\phi} = -j\eta \frac{ka_2^2}{4r_2^2} I_2 e^{-j(\omega t + kr_2 + \phi)} \sin\theta_2$$

Table 1. Parameters of the proposed IPT setup

Parameters	Values
System operating frequency f	1 MHz
Angular frequency ω	6.2832×10^{6} rad/s
Primary current I_1 (peak)	10A
Turns $N_1=N_2$	1
Radii of two coils $a_1=a_2$	0.48m
Radii of two wires $b_1=b_2$	0.005m
Separation distance d	0.4m
Resistor load R_L	5Ω
Tuning capacitor C_s	9.05nF

- Field energy density of the electric field

$$\mathbf{E}_c = \begin{pmatrix} \sin\theta_1\cos\varphi & \cos\theta_1\cos\varphi & -\sin\varphi \\ \sin\theta_1\sin\varphi & \cos\theta_1\sin\varphi & \cos\varphi \\ \cos\theta_1 & -\sin\theta_1 & 0 \end{pmatrix} \cdot \mathbf{E}_1 + \begin{pmatrix} \sin\theta_2\cos\varphi & \cos\theta_2\cos\varphi & -\sin\varphi \\ \sin\theta_2\sin\varphi & \cos\theta_2\sin\varphi & \cos\varphi \\ \cos\theta_2 & -\sin\theta_2 & 0 \end{pmatrix} \cdot \mathbf{E}_2$$

$$u_E = \frac{1}{2}\varepsilon_0 \cdot \mathrm{Re}[\mathbf{E}_c]^2$$

- Field energy density of the magnetic field

$$\mathbf{H}_c = \begin{pmatrix} \sin\theta_1\cos\varphi & \cos\theta_1\cos\varphi & -\sin\varphi \\ \sin\theta_1\sin\varphi & \cos\theta_1\sin\varphi & \cos\varphi \\ \cos\theta_1 & -\sin\theta_1 & 0 \end{pmatrix} \cdot \mathbf{H}_1 + \begin{pmatrix} \sin\theta_2\cos\varphi & \cos\theta_2\cos\varphi & -\sin\varphi \\ \sin\theta_2\sin\varphi & \cos\theta_2\sin\varphi & \cos\varphi \\ \cos\theta_2 & -\sin\theta_2 & 0 \end{pmatrix} \cdot \mathbf{H}_2$$

$$u_H = \frac{1}{2}\mu_0 \cdot \mathrm{Re}[\mathbf{H}_c]^2$$

Analysis of field density distribution

- Magnetic field distribution (open)

$$\vec{B}_x = \vec{B}_{x1} + \vec{B}_{x2} = \mathrm{Re}\left[\frac{\mu_0 (i_1 + i_2) a}{4\pi} \int_0^{2\pi} \frac{z\cos\theta}{\left[x^2 + y^2 + z^2 + a^2 - 2a(x\cos\theta + y\sin\theta)\right]^{3/2}} \mathrm{d}\theta\right]$$

$$\vec{B}_y = \vec{B}_{y1} + \vec{B}_{y2} = \mathrm{Re}\left[\frac{\mu_0 (i_1 + i_2) a}{4\pi} \int_0^{2\pi} \frac{z\sin\theta}{\left[x^2 + y^2 + z^2 + a^2 - 2a(x\cos\theta + y\sin\theta)\right]^{3/2}} \mathrm{d}\theta\right]$$

$$\vec{B}_z = \vec{B}_{z1} + \vec{B}_{z2} = \mathrm{Re}\left[\frac{\mu_0 (i_1 + i_2) a}{4\pi} \int_0^{2\pi} \frac{a - x\cos\theta}{\left[x^2 + y^2 + z^2 + a^2 - 2a(x\cos\theta + y\sin\theta)\right]^{3/2}} \mathrm{d}\theta\right]$$

- Electric field distribution (open)

$$\vec{E}_x = \vec{E}_{x1} + \vec{E}_{x2} = \mathrm{Re}\left[-j\omega \frac{\mu_0 (i_1 + i_2) a}{4\pi} \int_0^{2\pi} \frac{-\sin\theta}{\sqrt{x^2 + y^2 + z^2 + a^2 - 2a(x\cos\theta + y\sin\theta)}} \mathrm{d}\theta\right]$$

$$\vec{E}_y = \vec{E}_{y1} + \vec{E}_{y2} = \mathrm{Re}\left[-j\omega \frac{\mu_0 (i_1 + i_2) a}{4\pi} \int_0^{2\pi} \frac{\cos\theta}{\sqrt{x^2 + y^2 + z^2 + a^2 - 2a(x\cos\theta + y\sin\theta)}} \mathrm{d}\theta\right]$$

$$\vec{E}_z = \vec{E}_{z1} + \vec{E}_{z2} = 0$$

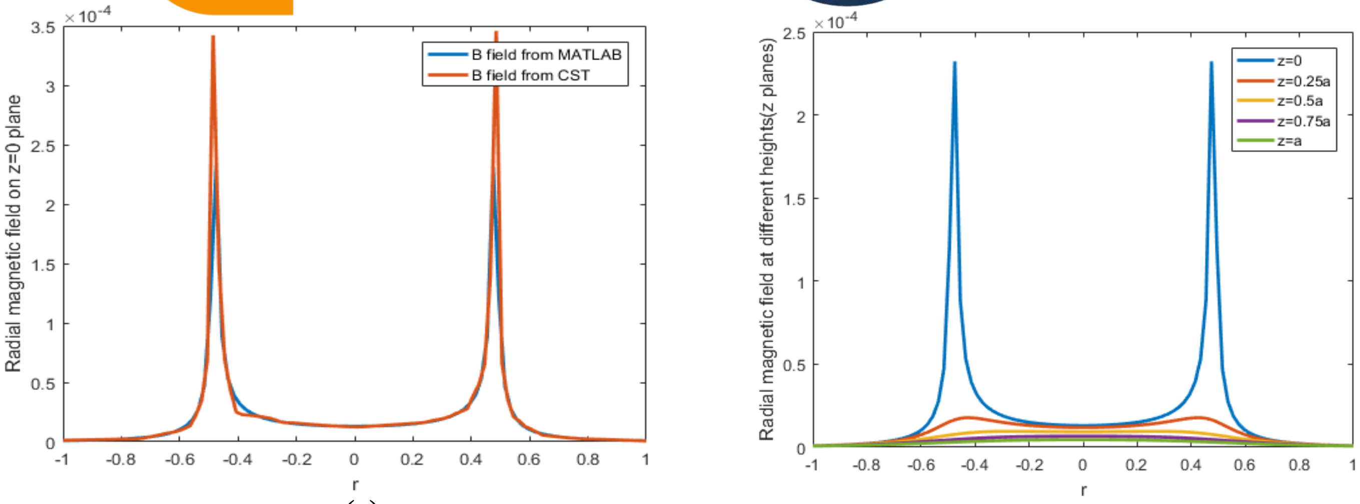

(a) (b)

Fig. 11 (a) Magnetic field of the primary coil along the radial direction the from MATLAB and CST, (b) Magnetic field of the primary coil along the radial direction at different z-heights

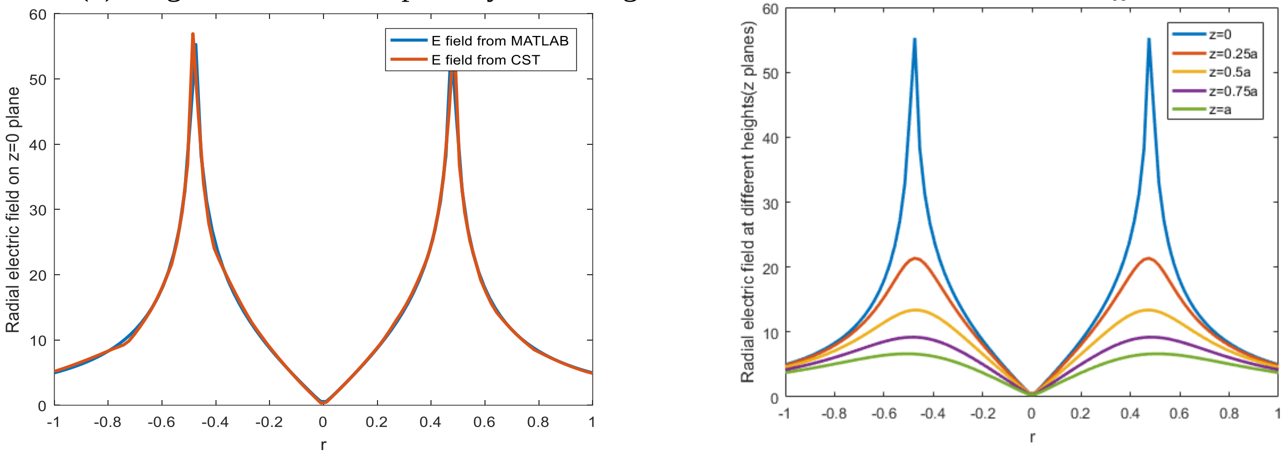

(a) (b)

Fig. 12 (a) Electric field of the primary coil along the radial direction the from MATLAB and CST, (b) Electric field of the primary coil along the radial direction at different z-heights

Analysis of field density distribution

- Magnetic field distribution (loaded)

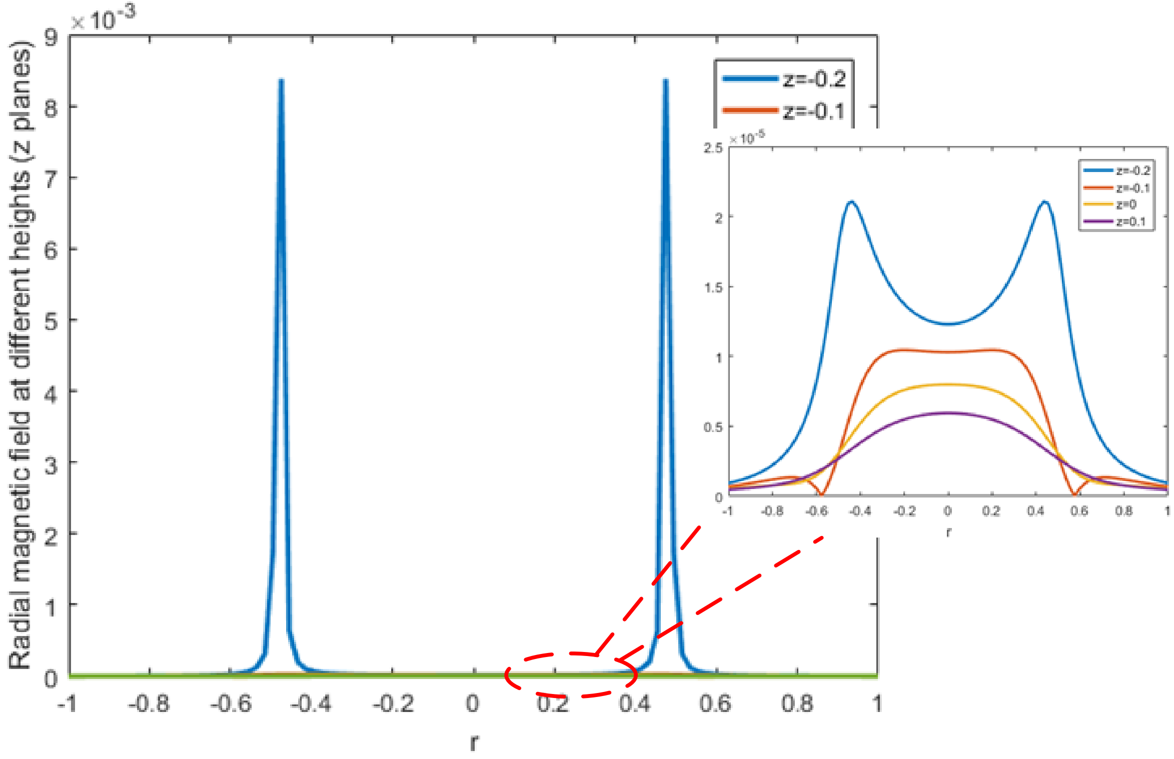

Fig. 13 Radial magnetic field at different z heights between two coils

- Electric field distribution (loaded)

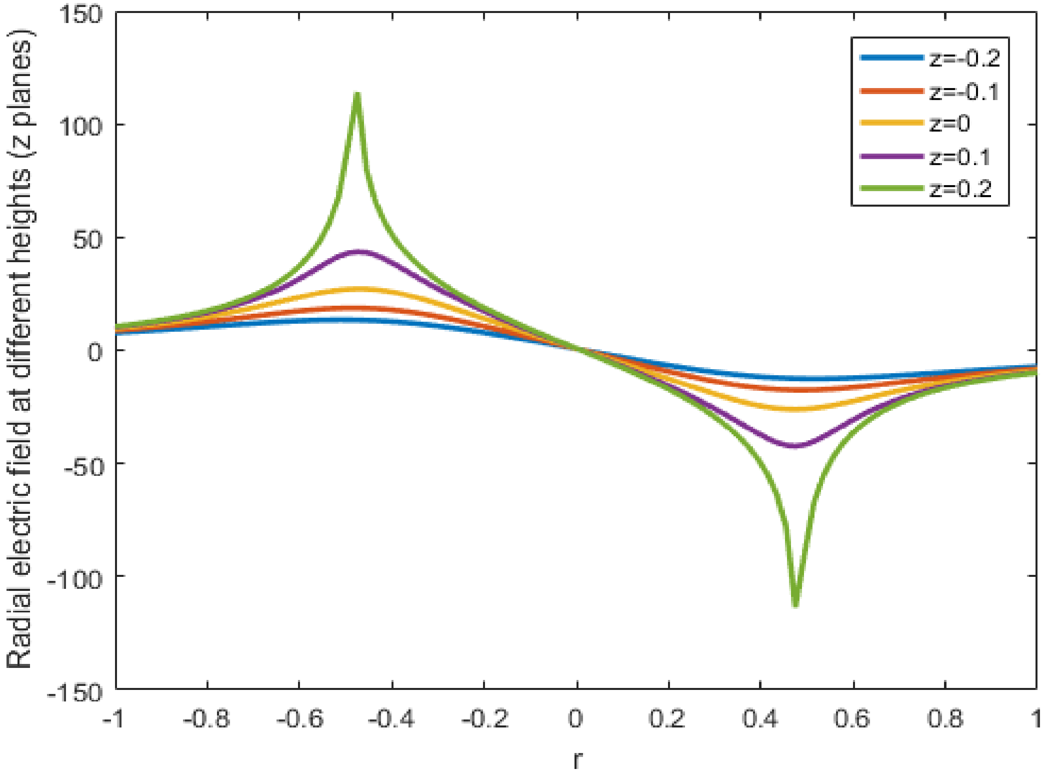

Fig. 14 Radial electric field between two coils at different z heights

Analysis of field density distribution

- Field energy density distribution (open)

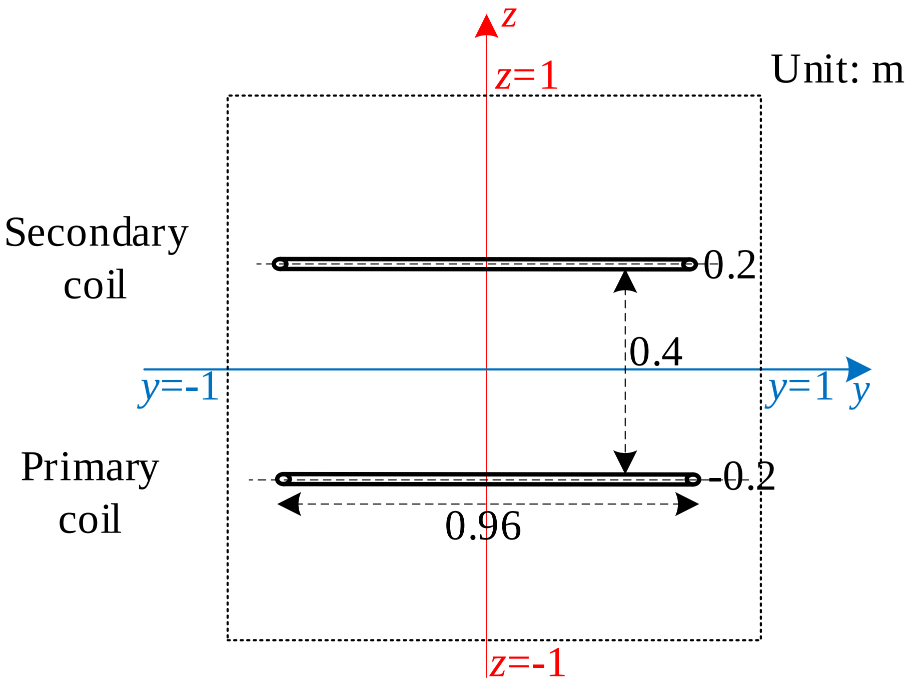

Fig. 15 Calculated region of field energy density distribution in the yoz plane

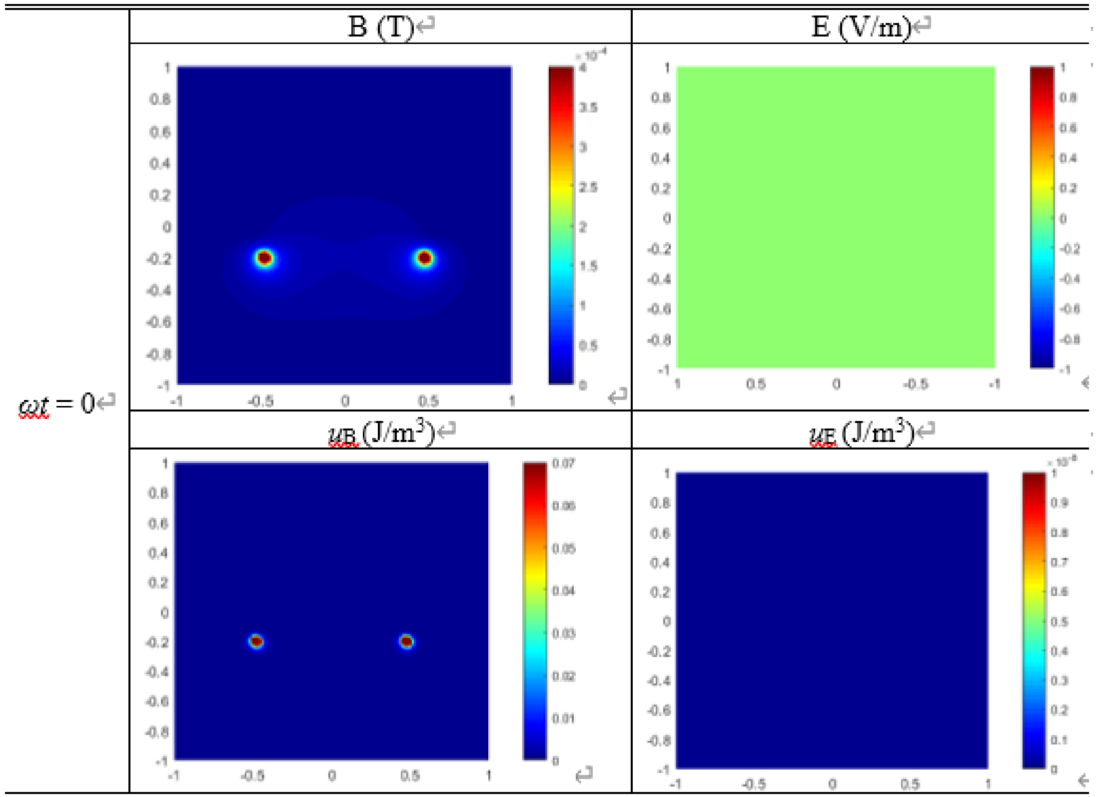

(a)

Analysis of field density distribution

- Field energy density distribution (loaded)

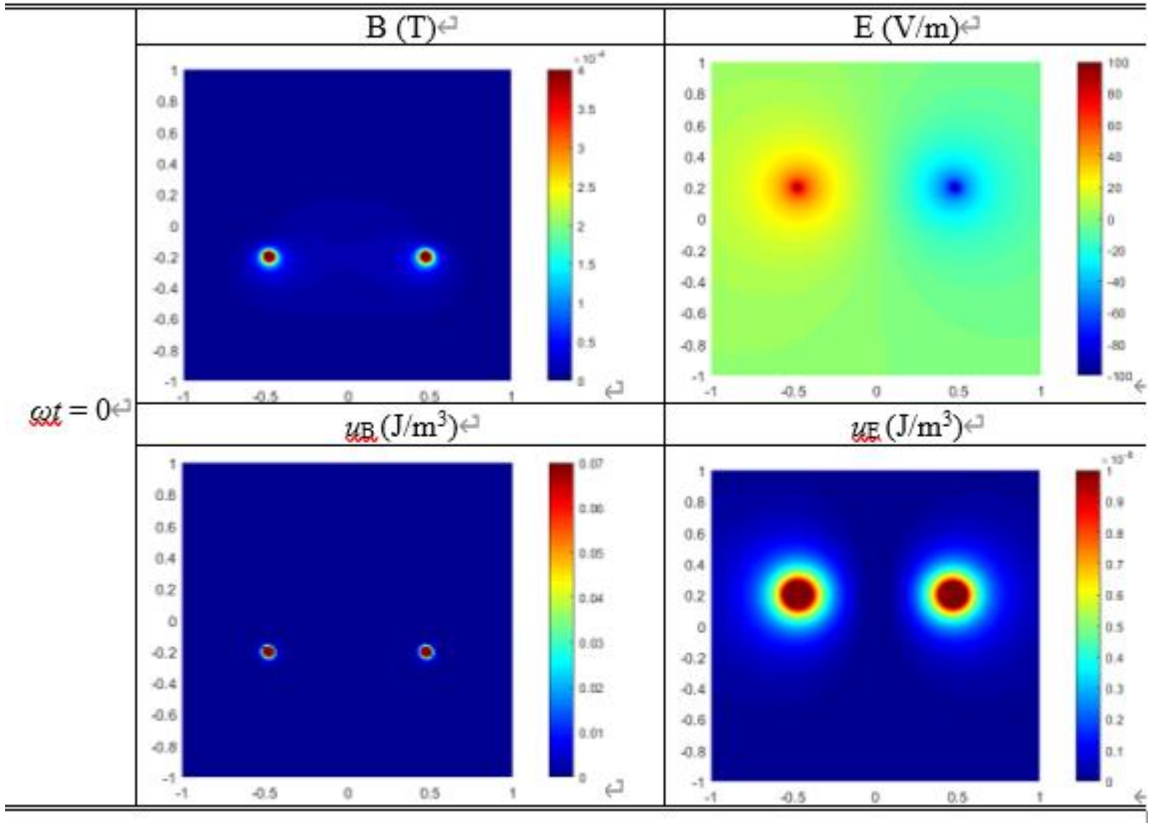

(a)

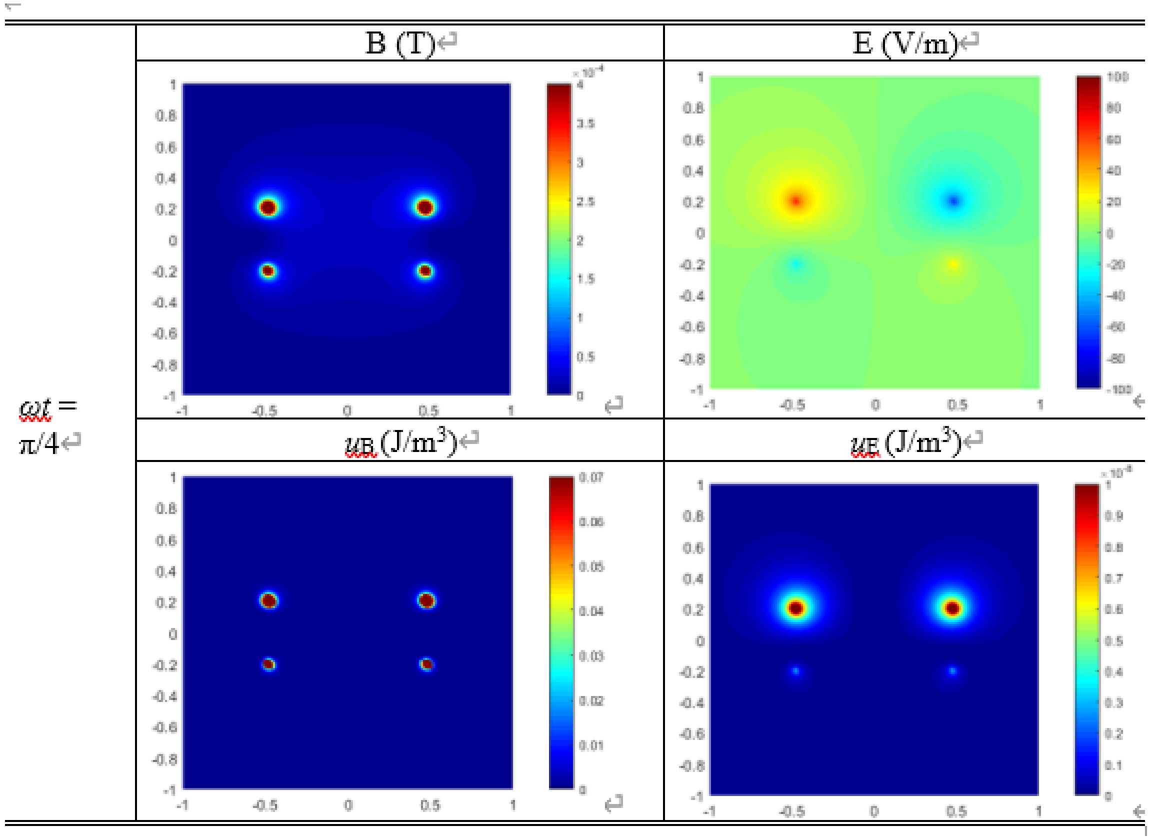

(b)

Analysis of field density distribution

- Field energy density distribution (loaded)

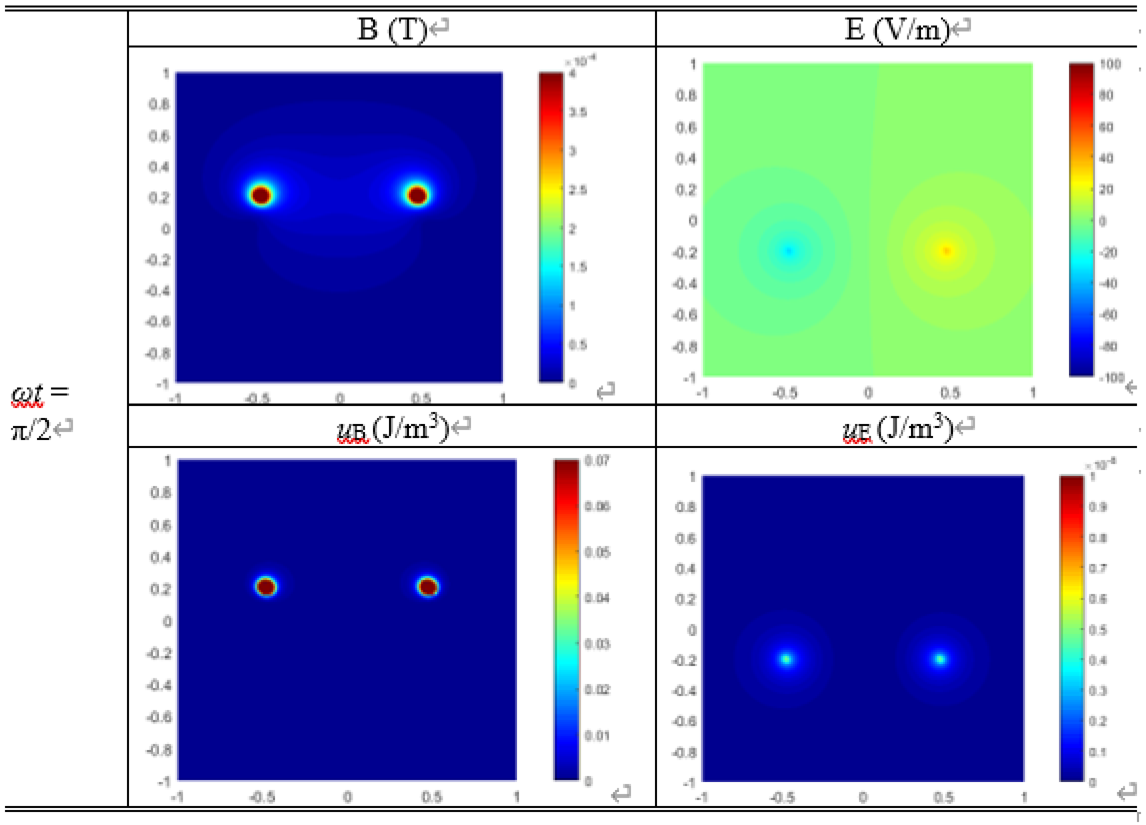

(c)

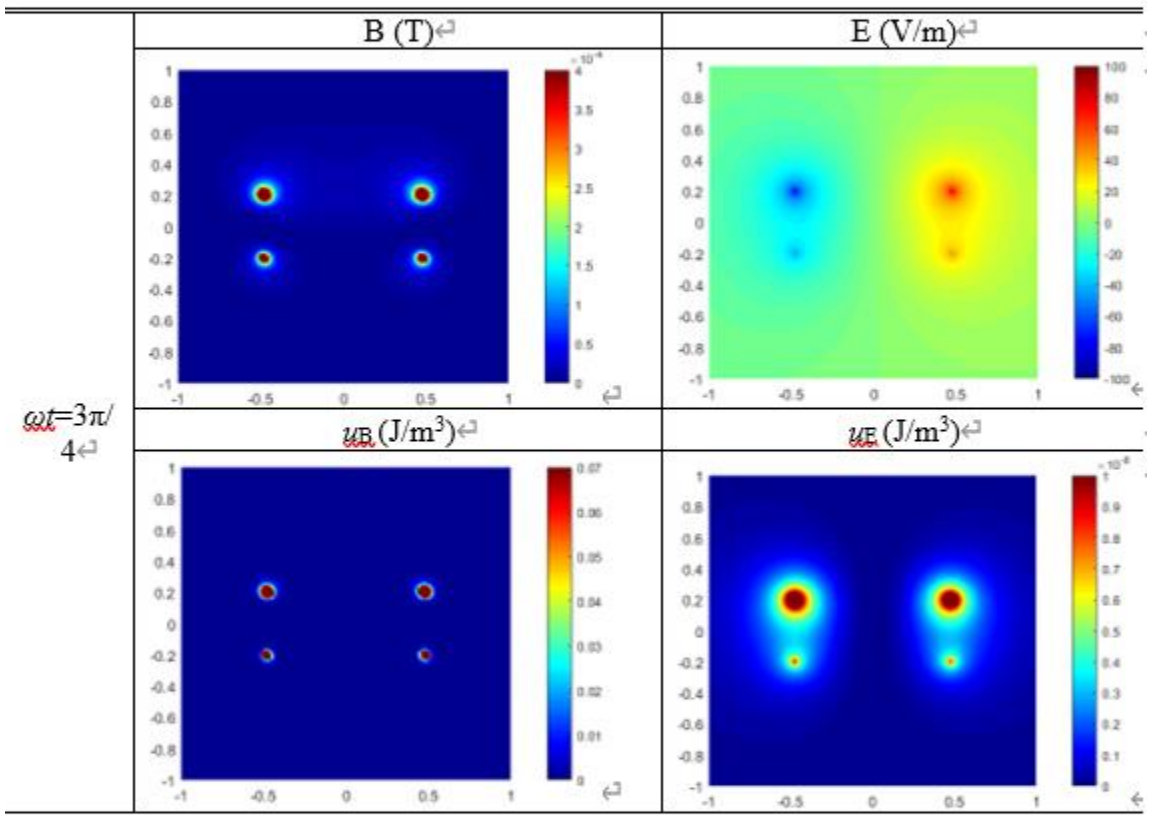

(d)

Fig. 16 Time sequence of field and field energy density distribution for the 2D system with a loaded secondary. (a) ωt = 0, (b) ωt = π/4, (c) ωt = π/2, (d) ωt = 3π/4

Active Power by Poynting vector

- B and E field at an arbitrary point between and around two coupled coils

$$\mathbf{H_1} = H_{1r}\vec{r}_1 + H_{1\theta}\vec{\theta}_1$$

$$H_{1r} = \frac{ka_1^2}{2}\left(\frac{j}{r_1^2} + \frac{1}{kr_1^3}\right)\hat{I}_1 e^{-j(\omega t + kr_1)}\cos\theta_1$$

$$H_{1\theta} = -\frac{(ka_1)^2}{4}\left(\frac{1}{r_1} + \frac{1}{jkr_1^2} - \frac{1}{k^2 r_1^3}\right)\hat{I}_1 e^{-j(\omega t + kr_1)}\sin\theta_1$$

$$\mathbf{H}_2 = H_{2r}\vec{r}_2 + H_{2\theta}\vec{\theta}_2$$

$$H_{2r} = \frac{ka_2^2}{2}\left(\frac{j}{r_2^2} + \frac{1}{kr_2^3}\right)\hat{I}_2 e^{-j(\omega t + kr_2 + \phi)}\cos\theta_2$$

$$H_{2\theta} = -\frac{(ka_2)^2}{4}\left(\frac{1}{r_2} + \frac{1}{jkr_2^2} - \frac{1}{k^2 r_2^3}\right)\hat{I}_2 e^{-j(\omega t + kr_2 + \phi)}\sin\theta_2$$

$$\mathbf{E_1} = E_{1\varphi}\vec{\varphi}$$

$$E_{1\varphi} = \eta\frac{(ka_1)^2}{4}\left(\frac{1}{r_1} + \frac{1}{jkr_1^2}\right)\hat{I}_1 e^{-j(\omega t + kr_1)}\sin\theta_1$$

$$\mathbf{E_2} = E_{2\varphi}\vec{\varphi}$$

$$E_{2\varphi} = \eta\frac{(ka_2)^2}{4}\left(\frac{1}{r_2} + \frac{1}{jkr_2^2}\right)\hat{I}_2 e^{-j(\omega t + kr_2 + \phi)}\sin\theta_2$$

Note: $\vec{r}_i$ $\vec{\theta}_i$ and $\vec{\varphi}$ are the orthogonal unit vectors in the directions of r_i, θ_i and φ in the spherical coordinates.

The unit vector $\vec{\boldsymbol{r}}_{\boldsymbol{i}}$ represents the direction in which the radial distance from the centre of two coils increases,

$\vec{\theta}_i$ represents the direction in which the angle from the positive z-axis is increasing,

$\vec{\varphi}$ represents the direction in which the angle in the xy plane counter clockwise from the positive x-axis is increasing.

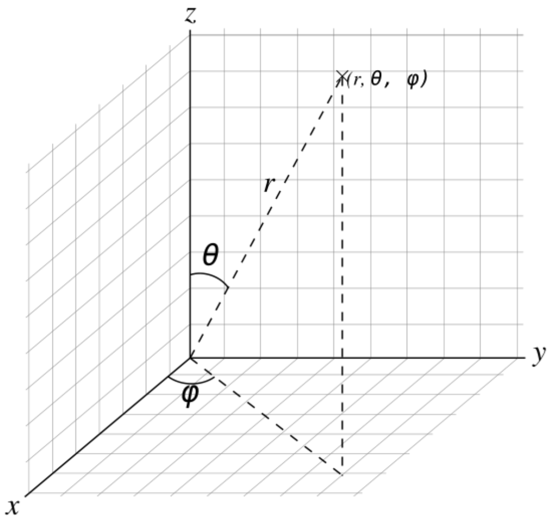

Active Power by Poynting vector

- Poynting vector at an arbitrary point between and around two coupled coils

The time-averaged Poynting vector **S**, by its definition as the half of the cross-product of **E** and conjugate **H** (**H***), is

$$\mathbf{S} = \boxed{\mathbf{S}_1} + \boxed{\mathbf{S}_2} + \boxed{\mathbf{S}_{12} + \mathbf{S}_{21}}$$

Contributed by the primary only (E1 x H1*)

Contributed by the secondary only (E2 x H2*)

The cross components $\mathbf{S}_{12}$ (E1 x H2*) and $\mathbf{S}_{21}$ (E2 x H1*) by interaction between two coils

$$\mathbf{S}_1 = \cancel{\frac{1}{2}\mathrm{Re}(\mathbf{E}_1 \times \mathbf{H}_1^*)} = 0$$

$$\mathbf{S}_2 = \cancel{\frac{1}{2}\mathrm{Re}(\mathbf{E}_2 \times \mathbf{H}_2^*)} = 0$$

The majority of IPT system running frequencies range from tens of kHz up to 13.56 MHz, so the wavenumber k (k= ω/c) is much less than 1 in IPT systems

$$\mathbf{S}_{12} = \frac{1}{2}\mathrm{Re}(\mathbf{E}_1 \times \mathbf{H}_2^*) = \frac{1}{2}\mathrm{Re}(-\mathbf{E}_{1\phi} \cdot \mathbf{H}_{2\theta}^*)\vec{r}_2 + \frac{1}{2}\mathrm{Re}(\mathbf{E}_{1\phi} \cdot \mathbf{H}_{2r}^*)\vec{\theta}_2$$

$$\mathbf{S}_{12r_2} = -\alpha \cdot \sin\theta_2 \cdot \sin(kr_2 - kr_1 + \phi)$$

$$\mathbf{S}_{12\theta_2} = \alpha \cdot 2\cos\theta_2 \cdot \sin(-kr_1 + kr_2 + \phi)$$

$$\mathbf{S}_{21} = \frac{1}{2}\mathrm{Re}(\mathbf{E}_2 \times \mathbf{H}_1^*) = \frac{1}{2}\mathrm{Re}(-\mathbf{E}_{2\phi} \cdot \mathbf{H}_{1\theta}^*)\vec{r}_1 + \frac{1}{2}\mathrm{Re}(\mathbf{E}_{2\phi} \cdot \mathbf{H}_{1r}^*)\vec{\theta}_1$$

$$\mathbf{S}_{21r} = -\alpha \cdot \sin\theta_1 \cdot \sin(\phi - kr_1 + kr_2)$$

$$\mathbf{S}_{21\theta_1} = \alpha \cdot 2\cos\theta_1 \cdot \sin(\phi - kr_1 + kr_2)$$

$$\textit{where} \quad \alpha = \frac{\eta k a_1^2 a_2^2 \hat{I}_1 \hat{I}_2 \sin\theta_1}{32 r_1^2 r_2^3}$$

Active Power by Poynting vector

- Poynting vector at an arbitrary point between and around two coupled coils

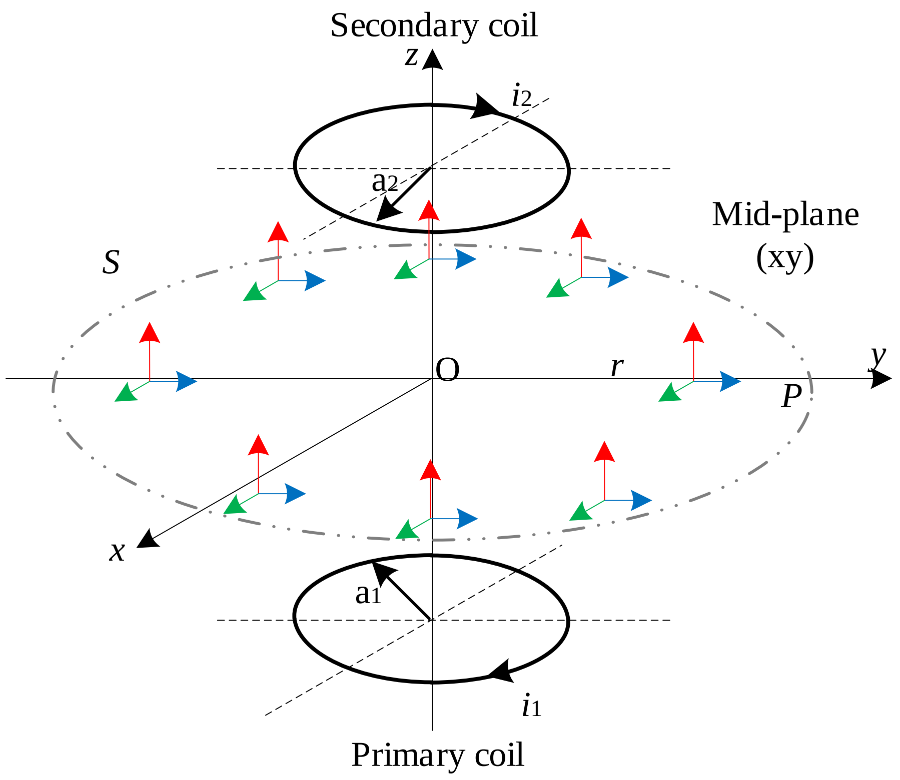

Fig.17 . Poynting vector distribution sketch in the xy mid-plane.

The selected point P is in the xy plane along the y axis, and r is the distance between P and the origin, which indicates the radius of the mid-plane.

The Poynting vector in the middle xy plane

$$\mathbf{S} = \left(0,\ 0,\ k\eta a_1^2 a_2^2 \hat{I}_1 \hat{I}_2 \sin\phi \frac{24dr^2}{(d^2+4r^2)^4}\right)$$

$$\sin\theta_i = r / r_i,$$
$$\cos\theta_i = (-1)^{i-1} d / 2r_i,$$
$$r_i = \sqrt{r^2 + (d/2)^2},\ i \in \{1, 2\},$$
$$\varphi \in [0, 2\pi);$$

To determine the power transfer, the z component has been integrated across the mid-plane between the two coupled coils,

$$P = \int_{-\infty}^{\infty} \mathbf{S} \cdot \vec{n} \cdot A d\sigma = k\eta a_1^2 a_2^2 \hat{I}_1 \hat{I}_2 \sin\phi \int_0^{\infty} \frac{24dr^2}{(d^2+4r^2)^4} \cdot 2\pi r dr$$

$$= \boxed{\frac{\omega\mu_0 \pi a_1^2 a_2^2 \hat{I}_1 \hat{I}_2 \sin\phi}{4d^3}}$$

where $k\eta = \omega\mu_0$, μ_0 and ε_0 are the magnetic permeability and electric permeability in vacuum

$$\boxed{P = \omega M I_1 I_2 \sin\phi}$$

Same result by the lumped circuit theory

- M is the mutual inductance between the two-coupled single turn circular coils
- I_1 and I_2 are RMS values of the currents in both the primary and secondary coil
- ϕ is the phase of the secondary current lagging that of the primary current

Active Power by Poynting vector

- Example power flow analysis

Table 2 Parameters of the proposed IPT setup

Parameters	Values
System operating frequency f	1 MHz
Angular frequencyω	6.2832×10^6 rad/s
Primary current I_1 (peak)	10A
Turns N_1=N_2	1
Radii of two coils a_1=a_2	0.48m
Radii of two wires b_1=b_2	0.005m
Separation distance d	0.4m
Resistor load R_L	5Ω

$$L = 0.01595 \cdot 2a \cdot [2.303 \cdot \log_{10}(\frac{8 \cdot 2a}{2b}) - 2] = 2.8\ \mu H$$

$$\hat{I}_2 = \frac{j\omega M \hat{I}_1}{j\omega L_2 + R_L} = 5.6245\angle 15.87^\circ\ A$$

$$P_{in} = \frac{1}{2}\hat{I}_1^2 \cdot \mathrm{Re}[\,j\omega L_1 + \frac{\omega^2 M^2}{(j\omega L_2 + R_L)}] = 79.09\ \mathrm{W}$$

$$P_{out} = \frac{1}{2}\left|\frac{j\omega M \hat{I}_1}{j\omega L_2 + R_L}\right|^2 \cdot R_L = 79.09\ \mathrm{W}$$

$$P_m = \frac{\omega\mu_0 \pi a_1^2 a_2^2 \hat{I}_1 \hat{I}_2 \sin\phi}{4d^3} = 79.09\ \mathrm{W}$$

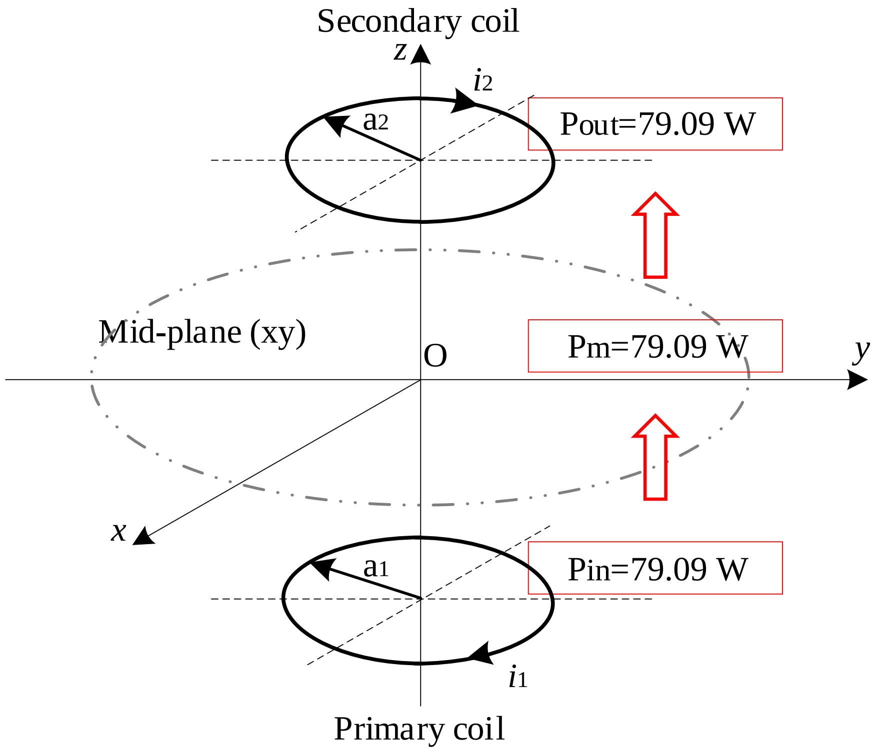

Fig.18. Input power, power across the mid-plane and output power of the example two-coil IPT system

Active Power by Poynting vector

- Power transfer channel and leakage analysis

Table 3 Active Power transferred of different channels and normalised percentage on mid-plane

Radius of power flow channel	Transferred power		Percentage	
	mid-plane	d/4 or 3d/4	mid-plane	d/4 or 3d/4
r=0	0	0	0	0
r=0.25a	13.68w	21.83w	0.173	0.276
r=0.5a	50.14w	55.52w	0.634	0.702
r=0.75a	67.94w	69.68w	0.859	0.881
r=a	74.42w	74.90w	0.941	0.947
r=1.25a	76.88w	77.03w	0.972	0.974
r=1.5a	77.9w	77.98w	0.985	0.986
r=1.75a	78.46w	78.46w	0.992	0.992
r=2a	78.7w	78.7w	0.995	0.995
r=2.25a	78.85w	78.85w	0.997	0.997
r=2.5a	78.93w	78.93w	0.998	0.998
r=2.75a	79.01w	79.01w	0.999	0.999
r=3a	79.01w	79.01w	0.999	0.999
……	……	……	1	1
$r \to \infty$	79.09w	79.09w	1	1

Active Power by Poynting vector

- Consistent active power transfer through different cross-sectional areas

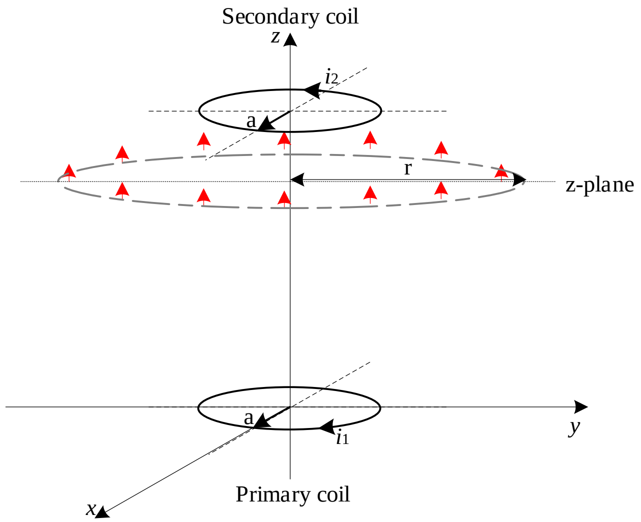

Fig. 19 A random selected cross-sectional z-plane to calculate the transferred active power

- If the selected point P is in the plane parallel to the xoy-plane and at the height of z, then the coordinate transformation from the spherical coordinate to the Cartesian coordinate is

$$\sin\theta_1 = r/r_1,\quad \cos\theta_1 = (x+d/2)/r_1,$$

$$\sin\theta_2 = r/r_2,\quad \cos\theta_1 = (x-d/2)/r_1,$$

$$r_1 = \sqrt{r^2+(x+d/2)^2},\quad r_2 = \sqrt{r^2+(d/2-x)^2},\quad \varphi \in [0, 2\pi);$$

- The Poynting vector in the selected plane could be simplified as in

$$\mathbf{S}_x = 0$$

$$\mathbf{S}_y = -\frac{4kr(d^4+2d^2(r^2-4z^2)-8(r^2-2z^2)(r^2+z^2))\eta\sin\phi a_1^2 a_2^2 I_1 I_2}{(4r^2+(d-2z)^2)^{5/2}(4r^2+(d+2z)^2)^{5/2}}$$

$$\mathbf{S}_z = \frac{24kr^2 z(-d^2+4(r^2+z^2))\eta\sin\phi a_1^2 a_2^2 I_1 I_2}{(4r^2+(d-2z)^2)^{5/2}(4r^2+(d+2z)^2)^{5/2}}$$

- The Power transfers across is

$$P = \int_{-\infty}^{\infty} S_z \cdot \vec{n} \cdot A d\sigma$$

$$= k\eta a_1^2 a_2^2 \hat{I}_1 \hat{I}_2 \sin\phi \int_0^{\infty} \frac{24r^2 z(-d^2+4(r^2+z^2))}{(4r^2+(d-2z)^2)^{5/2}(4r^2+(d+2z)^2)^{5/2}} \cdot 2\pi r dr$$

$$P = \omega M I_1 I_2 \sin\phi \Longleftrightarrow = \frac{k\eta a_1^2 a_2^2 \hat{I}_1 \hat{I}_2 \sin\phi (d-2z)\sqrt{(d-2z)^2}(1+\sqrt{\frac{1}{(d-2z)^2}}\sqrt{\frac{1}{(d+2z)^2}}(d^2-4z^2))}{8d^3\sqrt{(d-2x)^2}(d+2x)}$$

Poynting vector distribution

S_y, and S_z in the yz-plane from (4.10) are simplified as,

$$S_y = \alpha \cdot \frac{2\cos^2\theta_2 \sin\theta_1 r_1 - \sin\theta_1 \sin^2\theta_2 r_1 - 2\cos^2\theta_1 \sin\theta_2 r_2 + \sin^2\theta_1 \sin\theta_2 r_2}{r_1^3 r_2^3}$$

$$S_z = \alpha \cdot \frac{3\sin\theta_1 \sin\theta_2 \cos\theta_1 r_2 - 3\sin\theta_1 \sin\theta_2 \cos\theta_2 r_1}{r_1^3 r_2^3}$$

where $\alpha = \frac{k\eta a_1^2 a_2^2 \hat{I}_1 \hat{I}_2 \sin\phi}{32}$.

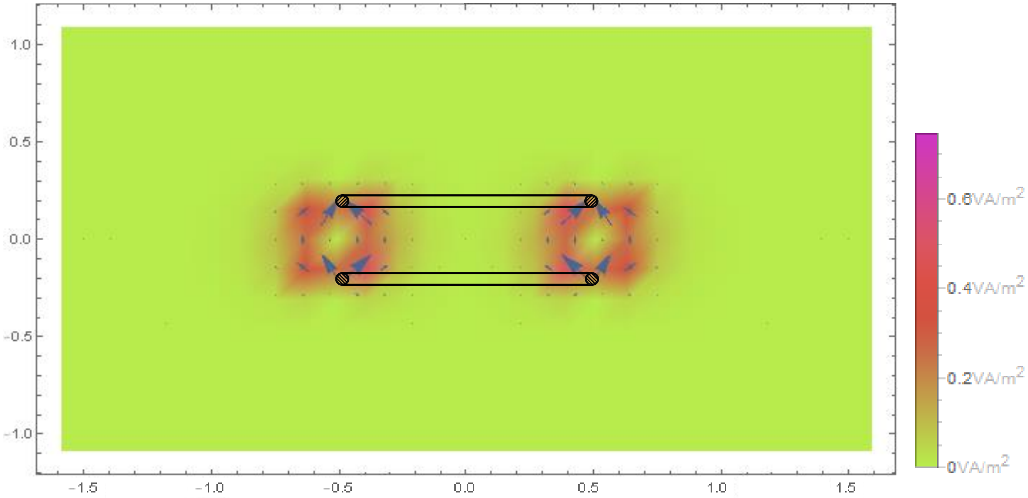

Fig. 20. Two-dimensional (2D) analytical result of the power distribution between the primary and secondary coil using *Mathematica*.

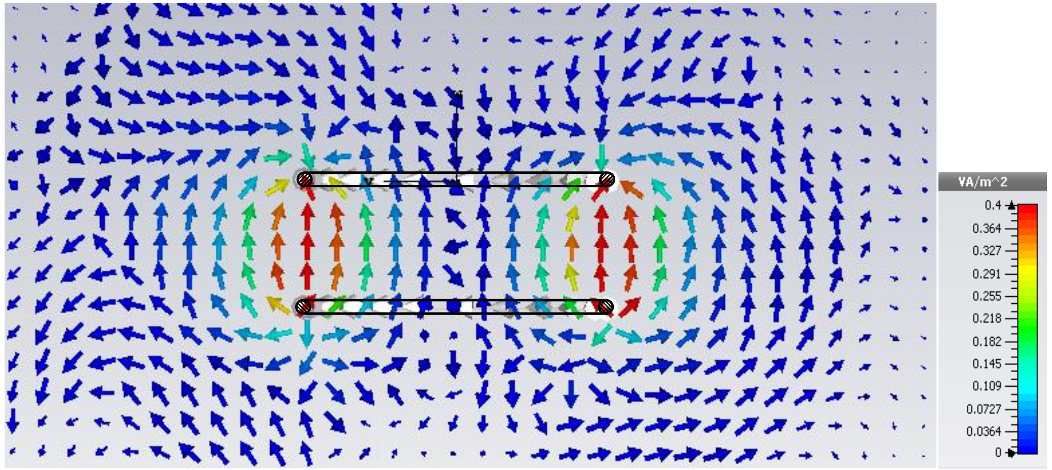

Fig. 21 Two-dimensional (2D) simulation result of the power distribution between the primary and secondary coil using Computer Simulation Technology (CST).

Reactive Power by Poynting vector

- Poynting vectors of open-circuited IPT system

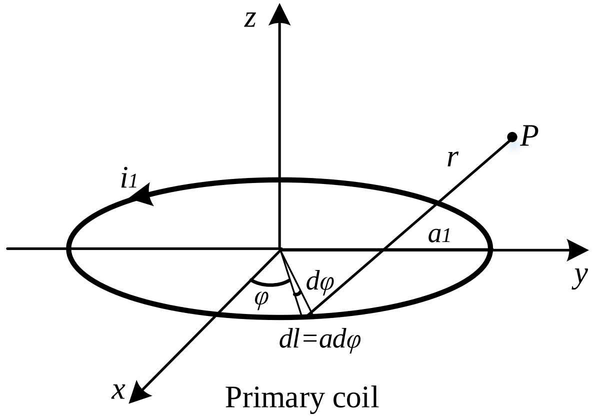

Fig. 23 The proposed open-circuited IPT system

$$\mathbf{B}_{(x,y,z)} = \frac{\mu_0 I e^{-j\omega t} a_1}{4\pi} \int_0^{2\pi} \frac{[0, z\sin\theta, a_1 - y\sin\theta]}{[y^2 + z^2 + a_1^2 - 2a_1 y \sin\theta)]^{\frac{3}{2}}} d\theta$$

$$\mathbf{E}_{(x,y,z)} = -j\omega \cdot \mathbf{A}_{(x,y,z)} = j\omega \frac{\mu_0 I e^{-j\omega t} a_1}{4\pi} \int_0^{2\pi} \frac{[\sin\theta, 0, 0]}{[y^2 + z^2 + a_1^2 - 2a_1 y \sin\theta)]^{\frac{1}{2}}} d\theta$$

$$\mathbf{S} = \mathbf{E}_{(x,y,z)} \times \mathbf{H}^*_{(x,y,z)}$$

$$\mathrm{Re}(\mathbf{S}) = 0$$

$$\mathrm{Im}(\mathbf{S}) = [0, -E_x \cdot \mathrm{H}_z^*, E_x \cdot \mathrm{H}_y^*]$$

$$S_y = j\frac{\omega\mu_0 I^2 a_1^2}{16\pi^2} \int_0^{2\pi} \frac{\sin\theta}{[y^2 + z^2 + a_1^2 - 2a_1 y \sin\theta)]^{\frac{1}{2}}} d\theta \cdot \int_0^{2\pi} \frac{a_1 - y\sin\theta}{[y^2 + z^2 + a_1^2 - 2a_1 y \sin\theta)]^{\frac{3}{2}}} d\theta$$

$$S_z = j\frac{\omega\mu_0 I^2 a_1^2}{16\pi^2} \int_0^{2\pi} \frac{\sin\theta}{[y^2 + z^2 + a_1^2 - 2a_1 y \sin\theta)]^{\frac{1}{2}}} d\theta \cdot \int_0^{2\pi} \frac{\mathrm{z}\sin\theta}{[y^2 + z^2 + a_1^2 - 2a_1 y \sin\theta)]^{\frac{3}{2}}} d\theta$$

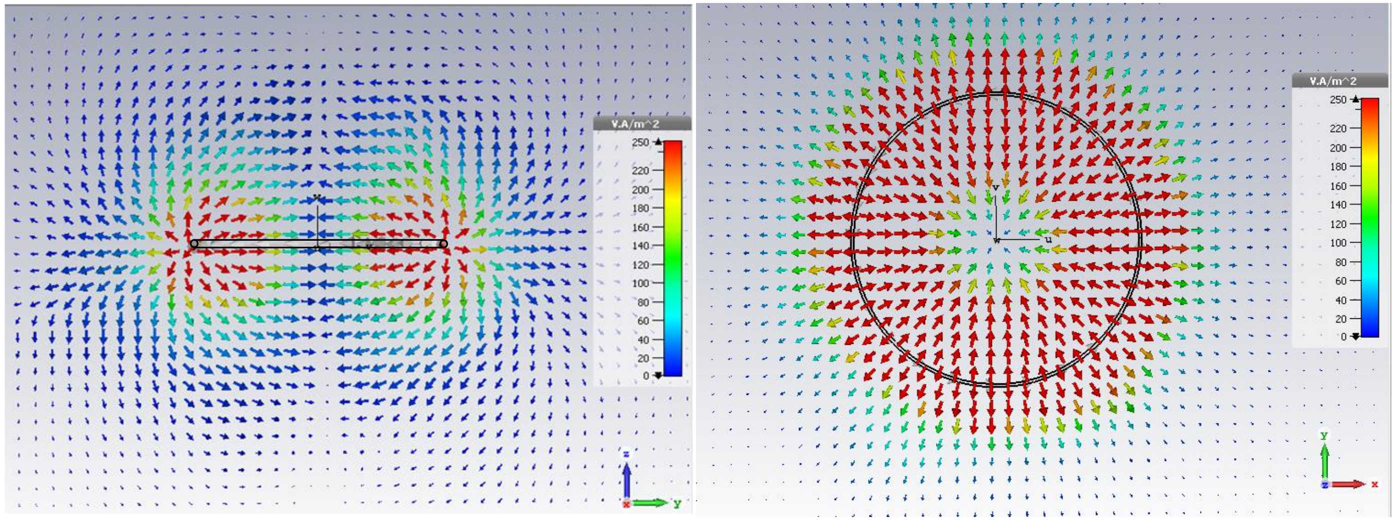

(a) (b)

Fig. 24 Imaginary components of Poynting vectors distribution of open secondary IPT system, Phase θ = 0. (a) front view, (b) top view.

Reactive Power by Poynting vector

- Integral surface selection and reactive power calculation

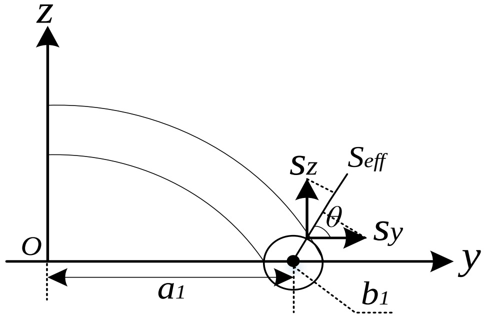

Fig. 25 The Poynting vector at a point on the primary coil cross-section (yoz plane)

$$S_{eff} = S_y \cdot \cos\theta + S_z \cdot \sin\theta$$

where $\cos\theta = \dfrac{y - a_1}{b_1}$ and $\sin\theta = \dfrac{z}{b_1}$

The average Poynting vector across the whole torus area is calculated to obtain the reactive power of the primary coil.

$$Q_{PR} = \iint_A S_{eff} \cdot dA = S_{eff} \cdot 4\pi^2 a_1 b_1$$

- Reactive power by circuit theory

$$L = 0.01595 \cdot 2a_1 \cdot [2.303 \cdot \log_{10}(\frac{8 \cdot 2a_1}{2b_1}) - 2] = 2.8\ \mu H$$

$$Q = \frac{1}{2}\omega L_1 \hat{I}_1^2 = 879.65 \text{ var}$$

Simulated Poynting vectors/reactive power
Calculated Poynting vector/reactive power

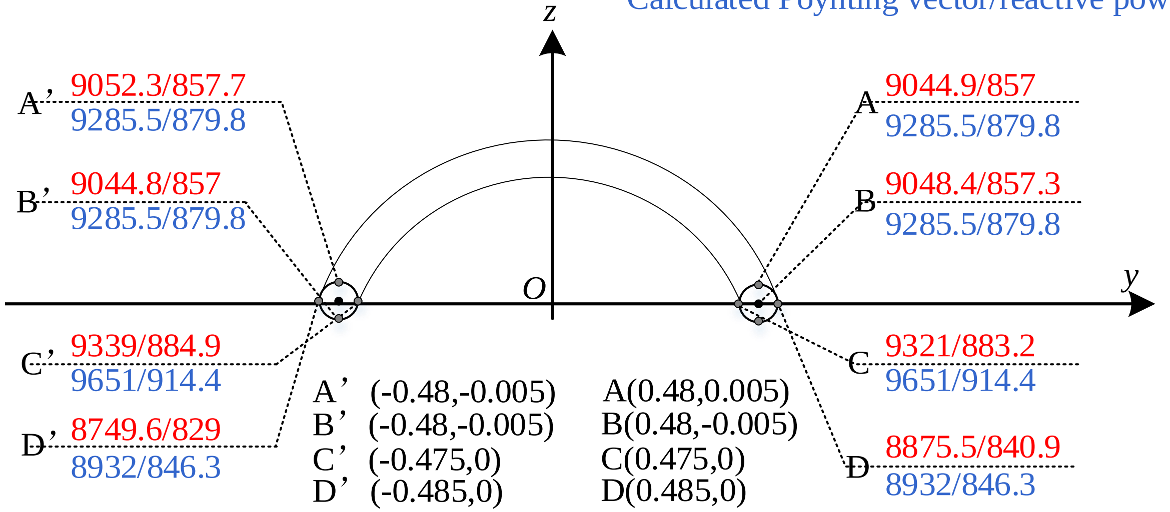

Fig. 26 Poynting vectors/reactive power at selected points on the primary coil

Table 4 Comparison between analytical and simulation results

	Poynting vector (var/m²)		Reactive power (var)		Error
	Analysed value	Simulated value	Analysed value	Simulated value	
A	9285.5	9044.88	879.8	856.99	0.026
B	9285.5	9048.38	879.8	857.32	0.026
C	9651	9320.97	914.41	883.15	0.044
D	8932	8875.46	846.31	840.93	0.006
A’	9285.5	9052.26	879.8	857.69	0.025
B’	9285.5	9044.79	879.8	856.98	0.026
C’	9651	9338.99	914.41	884.85	0.032
D’	8932	8749.6	846.31	829.01	0.002
Ave	9288.5	9059.42	880.08	858.36	0.025

Reactive Power by Poynting vector

- Poynting vector at an arbitrary point of a loaded system

The time-averaged Poynting vector **S**, by its definition as the half of the cross-product of **E** and conjugate **H** (**H***), now the imaginary part is calculated as

$$\mathbf{S} = \boxed{\mathbf{S}_1} + \boxed{\mathbf{S}_2} + \boxed{\mathbf{S}_{12} + \mathbf{S}_{21}}$$

Contributed by the primary only (E1 x H1*)

Contributed by the secondary only (E2 x H2*)

The cross components $\mathbf{S}_{12}$ (E1 x H2*) and $\mathbf{S}_{21}$ (E2 x H1*) by interaction between two coils

$$\mathbf{S}_{11} = \frac{1}{2}\mathbf{E}_1 \times \mathbf{H}_1^* = 0 + j\mathbf{S}_{11I}$$

$$\mathbf{S}_{22} = \frac{1}{2}\mathbf{E}_2 \times \mathbf{H}_2^* = 0 + j\mathbf{S}_{22I}$$

$$\mathbf{S}_{12} = \frac{1}{2}\mathbf{E}_1 \times \mathbf{H}_2^* = \frac{1}{2}(-\mathbf{E}_{1\phi} \cdot \mathbf{H}_{2\theta}^*)\vec{r}_2 + \frac{1}{2}(\mathbf{E}_{1\phi} \cdot \mathbf{H}_{2r}^*)\vec{\theta}_2 = \mathbf{S}_{12R} + j\mathbf{S}_{12I}$$

$$\text{where } \mathbf{S}_{12I} = \frac{k\eta a_1^2 a_2^2 \hat{I}_1 \hat{I}_2}{16 r_1^2 r_2^3} \cos\phi \sin\theta_1 [\frac{\sin\theta_2}{2}, -\cos\theta_2, 0]$$

$$\mathbf{S}_{21} = \frac{1}{2}\mathbf{E}_2 \times \mathbf{H}_1^* = \frac{1}{2}(-\mathbf{E}_{2\phi} \cdot \mathbf{H}_{1\theta}^*)\vec{r}_1 + \frac{1}{2}(\mathbf{E}_{2\phi} \cdot \mathbf{H}_{1r}^*)\vec{\theta}_1 = \mathbf{S}_{21R} + j\mathbf{S}_{21I}$$

$$\text{where } \mathbf{S}_{21I} = \frac{k\eta a_1^2 a_2^2 \hat{I}_1 \hat{I}_2}{16 r_1^3 r_2^2} \cos\phi \sin\theta_2 [\frac{\sin\theta_1}{2}, -\cos\theta_1, 0]$$

Reactive Power by Poynting vector

- Reactive power of the primary in a loaded system

After the transformation of coordinates, a plane infinitely close to the primary coil is selected, and the imaginary parts of the z component of the mutual-Poynting vectors

$$\mathbf{S}_{21I\_z} = 0$$

$$\mathbf{S}_{12I\_z} = \frac{-3dk\eta\cos\phi a_1^2 a_1^2 I_1 I_2}{16r(d^2+r^2)^{5/2}}$$

$$Q_{21} = 0$$

$$Q_{12} = \int_A \mathbf{S}'_{12I\_z} \cdot 2\pi r dr$$

$$= \int_{r=0}^{+\infty} -\frac{3dk\eta\cos\phi a_1^2 a_1^2 I_1 I_2}{16r(d^2+r^2)^{5/2}} \cdot 2\pi r dr = -\frac{k\pi\eta\cos\phi a_1^2 a_1^2 I_1 I_2}{4d^3}$$

The reactive power supplied by the current flowing in the primary coil is equal to the integral of the self-Poynting vector $\mathbf{S}_{11I}$ over the closed torus of the primary coil,

$$Q_{11} = \iint_A S_{11I\_eff} \cdot dA = S_{11I\_eff} \cdot 4\pi^2 a_1 b_1 = 880.08 \text{ var}$$

Plus the reactive power by integral of the mutual-Poynting vectors over the infinity plane which is close to the primary coil, $Q_{12} = \iint_A S'_{12I\_z} dA = \int_0^{\infty} S'_{12I\_z} \cdot 2\pi r dr = -284.38 \text{ var}$

$$\boxed{Q = Q_{11} + Q_{12} = 595.7 \text{ var}}$$

- Validation by circuit theory

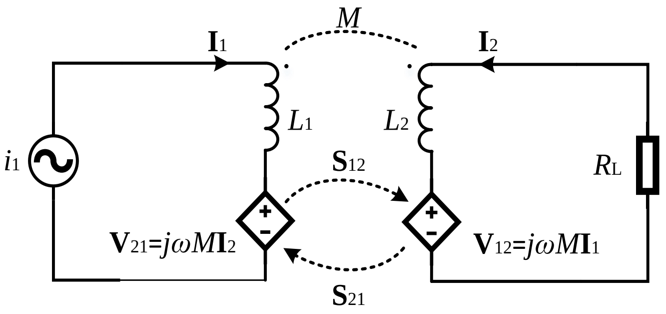

Fig. 27 Diagram of lumped circuit

$$Q = \mathrm{Im}[I_1^2 * j\omega L_1 + I_1^2 * \frac{\omega^2 M^2}{j\omega L_2 + R_L}]$$

$$= (879.65 - 290.64) \text{ var}$$

$$\boxed{= 589.01 \text{ var}}$$

Experimental Validation

- Equivalent circuit

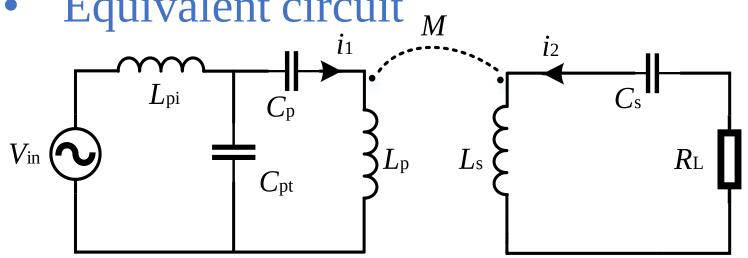

Fig. 28. Equivalent circuit of the practical IPT setup

Table 5 Parameters of the practical built IPT setup

Parameters	Values
System operating frequency f	1 MHz
Angular frequency ω	6.2832×10^6 rad/s
Primary current I_1 (peak)	3.8A
Turns $N_1=N_2$	1
Radii of two coils $a_1=a_2$	0.35m
Radii of two wires $b_1=b_2$	0.005m
Inductance of the primary coil	2.679µH
Inductance of the secondary coil	2.639µH
Primary tuning inductor L_{pi}	1µH
Primary tuning capacitor C_{pt}	34nF
Primary tuning capacitor C_p	14.51nF
Secondary tuning capacitor C_s	10.76nF
Separation distance d	0.175m
Lateral misalignment d'	0.105m
Resistor load R_L	1.3Ω
Litz wire	4 turns (4-mm diameter)

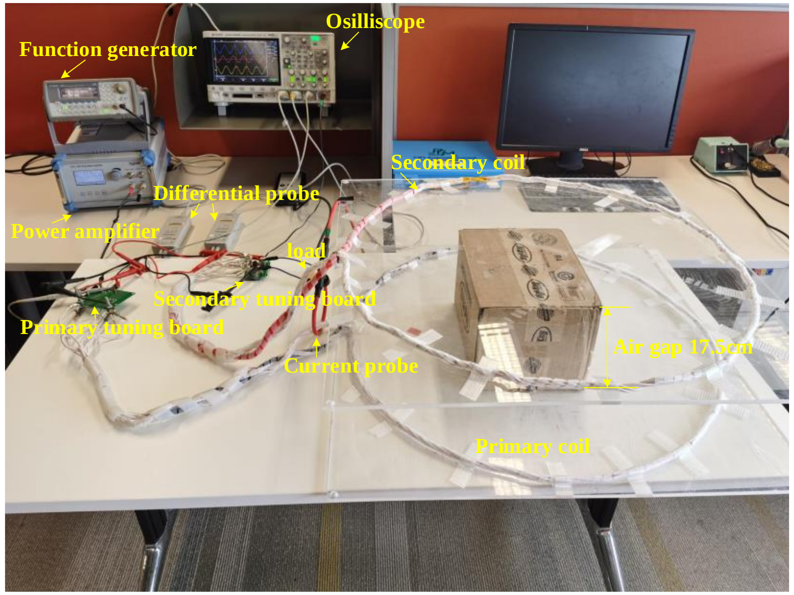

Fig. 29 Practical demonstration of the IPT setup with good alignment

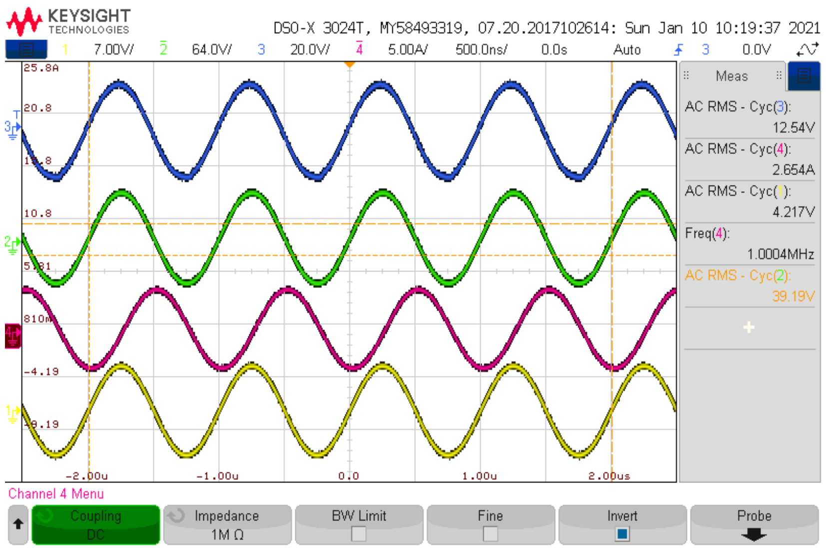

Fig. 30 Waveforms of the IPT system with good alignment

Table 6 Results comparison of the IPT setup with two coils coaxially Aligned

	Open circuit			loaded		
	Poynting vector analysis	Circuit analysis	Experiment	Poynting vector analysis	Circuit analysis	Experiment
Active power (W)	0	0	0	1.72	1.75	1.66
Reactive power (var)	127.4	123.4	123.4	120.63	118.2	118.6

Experimental Validation

- Experimental results of the system with misalignment

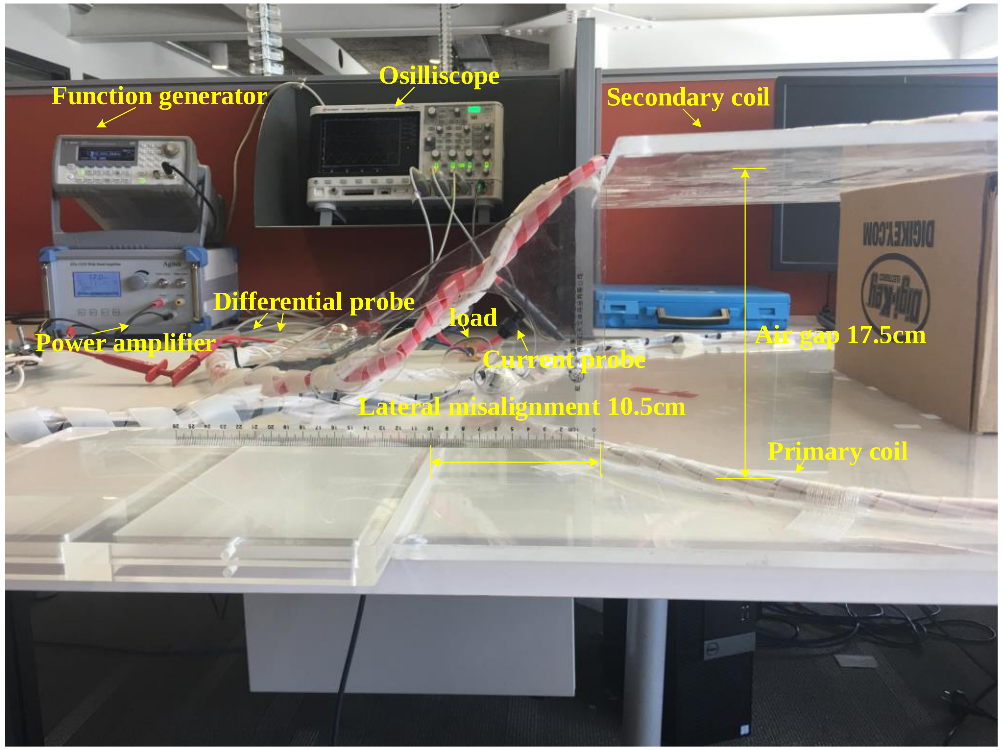

Fig. 31 Practical demonstration of the IPT setup with misalignment of 10.5cm

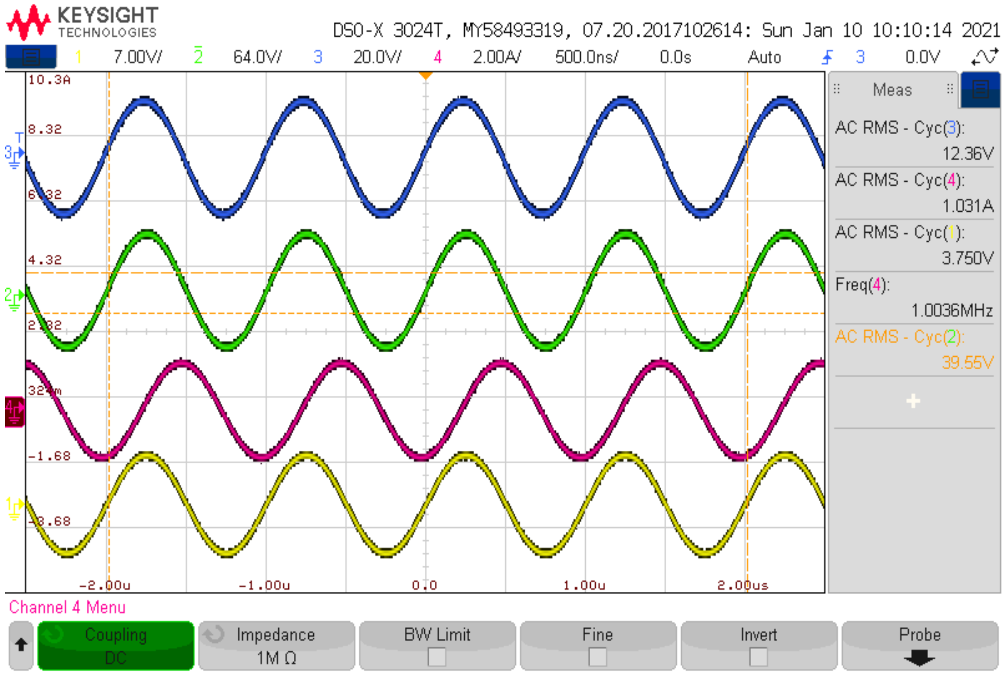

Fig. 32 Waveforms of the IPT system with misalignment of 10.5cm

Table 7 Results comparison of the IPT setup with two coils misaligned

	Open circuit			loaded		
	Poynting vector analysis	Circuit analysis	Experiment	Poynting vector analysis	Circuit analysis	Experiment
Active power (W)	0	0	0	1.51	1.5	1.38
Reactive power (var)	127.4	118.2	118.2	121.4	117.3	117.3

Publications

QuakeCoRE
NZ Centre for Earthquake Resilience
Te Hiranga Rū

Journal papers

[1] Liu, Yuan, and Aiguo Patrick Hu. "Investigation of Reactive Power Circulation between Two Coupled Coils of Inductively Coupled Wireless Power Transfer System by Poynting Vector Analysis", *International Journal of Electrical Power & Energy System*, DOI: 10.1016/J.IJEPES.2021.107621.

[2] Liu, Yuan, and Aiguo Patrick Hu. "Study of power flow in an IPT system based on Poynting vector analysis." *Energies,* 11.1 (2018): 165, DOI: 10.3390/en11010165.

[3] L. J. Zou, Yuan Liu, Yu-gang Su, A. P. Hu, " Study of power flow mechanism of capacitive power transfer system based on Poynting vector analysis," *International Journal of Electrical Power & Energy System 134*, DOI: 10.1016/J.IJEPES.2021.107374.

[4] K. Zhang, X. Ren, Y. Liu, S. Hui, B. Song, “Analytical Solution and Experimental Validation of the Electromagnetic Field in an IPT System”, Applied Sciences, DOI: 10.3390/app9071323.

Conference Papers

[5] Liu, Yuan, Aiguo Patrick Hu, and Kehan Zhang. "Numerical Analysis of Reactive Power Distribution between Two Coupled Coils by Poynting Vector." *2020 IEEE PELS Workshop on Emerging Technologies: Wireless Power Transfer (WoW).* IEEE, 2020.

[6] Liu, Yuan, and Aiguo Patrick Hu. "Power density distribution analysis of an IPT system based on Poynting vector." *2017 IEEE 12th International Conference on Power Electronics and Drive Systems (PEDS).* IEEE, 2017.

[7] Liu, Yuan, Aiguo Patrick Hu, and Udaya Madawala. "Determining the power distribution between two coupled coils based on Poynting vector analysis." *2017 IEEE PELS Workshop on Emerging Technologies: Wireless Power Transfer (WoW)*. IEEE, 2017

[8] Liu, Yuan, Patrick Aiguo Hu, and Udaya K. Madawala. "Maximum power transfer and efficiency analysis of different inductive power transfer tuning topologies." *2015 IEEE 10th Conference on Industrial Electronics and Applications (ICIEA)*. IEEE, 2015.

Thank You!